PCMDI Report No. 53

PREDICTABILITY AND THE RELATIONSHIP BETWEEN SUBSEASONAL AND INTERANNUAL VARIABILITY DURING THE ASIAN SUMMER MONSOON

by

Kenneth R. Sperber[1], Julia M. Slingo[2] and H. Annamalai[2]

**[1]Program for Climate Model diagnosis and Intercomparison
Lawrence Livermore National Laboratory, Livermore, CA, USA**

**[2]Centre for Global Atmospheric Modelling, Dept. of Meteorology
University of Reading, UK**

July 1999

Predictability and the Relationship Between Subseasonal and Interannual Variability During the Asian Summer Monsoon

Kenneth R. Sperber[1], Julia M. Slingo[2] and H. Annamalai[2]

[1]PCMDI, Lawrence Livermore National Laboratory, Livermore, CA 94550
[2]Centre for Global Atmospheric Modelling, Department of Meteorology,
University of Reading, UK

Dr. Kenneth R. Sperber
Program for Climate Model Diagnosis and Intercomparison
Lawrence Livermore National Laboratory
P.O. Box 808, L-264
Livermore, CA 94550 USA

Ph: (925) 422-7720
Fax: (925) 422-7675
E-mail: sperber@space.llnl.gov

Abstract

The relationship between subseasonal and interannual variability of the Asian Summer Monsoon has been investigated through analysis of the dominant modes of variability in the 40-year NCEP/NCAR Reanalysis, with complementary satellite and surface based precipitation data. The hypothesis that the characteristics of monsoon subseasonal variability (i.e. weather regimes) are modulated on interannual timescales in a systematic and therefore predictable manner has been tested. The null hypothesis is that predictability of the seasonal mean monsoon behaviour requires only that the effects of the slowly varying components of the climate system be correctly simulated.

An interannual mode of monsoon variability has been identified which is closely related to the observed seasonal mean all-India Rainfall (AIR). A counterpart of this mode has also been identified at subseasonal timescales which projects strongly on to the daily AIR, confirming that a common mode of monsoon variability exists on seasonal and subseasonal timescales.

It has been shown that the temporal behaviour of this subseasonal mode, as described by the probability distribution function (PDF) of the principal component timeseries, does not show any evidence of bimodality, the shape of the PDF being Gaussian. Further, it has been shown that the mean of the PDF is systematically and significantly perturbed towards negative (positive) values in weak (strong) monsoon years as categorized in terms of the seasonal mean AIR. This translation in the mean of the PDF, rather than a change in shape of the PDF suggests that anomalous monsoons are not associated with changes in weather regimes. Further analysis has confirmed that low frequency modulation of the basic state is primarily responsible for these shifts in the subseasonal PDFs, supporting the null hypothesis that predictability of the seasonal mean monsoon requires only that the effects of the slowly varying components of the climate system be correctly simulated. Thus model improvements to reduce systematic errors in the mean simulation and the response to low frequency boundary forcing may improve the prospects for dynamical seasonal prediction.

However, the results have also shown that only a subset of the subseasonal modes are systematically perturbed either by ENSO or in weak vs. strong monsoon years, suggesting that predictability is likely to be limited by the chaotic, internal variability of the monsoon system.

Keywords: Asian Monsoon, Seasonal Predictability, Interannual Variability

1. Introduction

Summer monsoon rainfall is the life-blood of the agrarian societies of subtropical Asia. A late monsoon or a weak monsoon can have disastrous consequences for productivity of the crops upon which hundreds of millions of people rely for sustenance (Swaminathran 1987, Kiladis and Sinha 1991). Conversely, a strong monsoon can cause flood conditions that also result in the loss of thousands of lives (Swaminathran 1987). Since the days of Sir Gilbert Walker, predictability of the Indian monsoon has been a goal of the forecasting community. While statistical forecasts of gross measures of summer monsoon variability have been moderately successful (Krishna Kumar et al. 1995), particularly during periods of strong boundary forcing (e.g., El Niño/Southern Oscillation, ENSO), dynamical seasonal prediction of the Indian summer monsoon, and the Asian summer monsoon in general, has met with much less success (Brankovic and Palmer 1999). However, the benefits of dynamical seasonal prediction could be substantial since ensembles of forecasts can potentially yield information on (1) the probability of strong or weak monsoon, and (2) the regionality of the anomalous rainfall and circulation which statistical methods cannot "foreshadow." It is important therefore that we identify and understand the factors that may be limiting our current level of predictability.

Two possible explanations for this lack of predictability have been postulated. The first is that model errors in the mean monsoon simulation are still substantial enough that the signal being sought is smaller than the systematic bias. Also, as Sperber and Palmer (1996) have shown, the known teleconnection between all-India rainfall (AIR) and tropical sea surface temperature (SST), indicative of a link between the monsoon and ENSO, is not faithfully captured by GCMs, again possibly related to errors in the model's basic state. If, as Charney and Shukla (1981) have suggested, it is the low frequency boundary forcing (e.g., SST) that predisposes the monsoon system towards a dry or wet state, then there is a clear need to improve model simulations before any conclusive statements can be made about the dynamical seasonal predictability of the Asian summer monsoon (ASM).

The second possible explanation involves the role of intraseasonal variability and the suggestion that this introduces a chaotic element into the prediction of seasonal mean anomalies. During the established phase of the monsoon the circulation often undergoes significant variations with a pronounced northward excursion of the monsoon trough which brings the monsoon into an inactive (break) phase over India. The change in the precipitation distribution over India and southeast Asia between active and break phases of the monsoon is substantial (e.g., Webster et al. 1998), and it is therefore quite possible that intraseasonal variability could have a significant influence on the seasonal mean rainfall. Krishnamurti and

Bhalme (1976), Sikka (1980), and Gadgil and Asha (1992) presented observational evidence that years of below-normal rainfall over central India are characterized by prolonged breaks in Indian monsoon rainfall. Alternatively, years of near-normal or above-normal rainfall tend to be characterized by fewer breaks of shorter duration. Further support for this idea came from early modelling studies which suggested that the dominant modes of interannual and intraseasonal variability had a common structure associated with the latitudinal shift in the tropical convergence zone (TCZ) from its position over the equatorial Indian Ocean northwards over the Indian subcontinent (e.g., Fennessy and Shukla 1994; Ferranti et al. 1997). This similarity led Palmer (1994) to propose a paradigm in which intraseasonal variability is essentially chaotic, with the interannual variability being governed by the frequency of occurrence of the active (continental) versus the break (oceanic) regimes. Using the Lorenz (1963) model, Palmer (1994) showed that the probability of being in one regime of phase space or another is no longer equally probable in the presence of external forcing. Similarly, using a more complex model of monsoon intraseasonal variability, Webster et al. (1998) found the probability distribution function (PDF) of intraseasonal variability changed shape and became bimodal in the presence of El Niño-like forcing. These studies suggest that the influence of the boundary forcing (e.g., SST) is to bias the system towards more active or break regimes. If it is the case that the intraseasonal variability, even if inherently chaotic, can be influenced by the boundary forcing, then there is potential for predictability on the seasonal to interannual timescale, but in a probabilistic, not deterministic sense.

The purpose of this paper is to investigate intraseasonal (30-70 days) and higher frequency (5-30 days) variability and its relationship to interannual variability during the ASM. The hypothesis that the characteristics of monsoon subseasonal variability (i.e., the weather regimes) are modulated on interannual timescales in a systematic and therefore predictable manner will be tested. The null hypothesis is then that predictability of monsoon interannual variability requires only that the effects of the slowly varying components of the climate system be correctly simulated.

Annamalai et al. (1999) made a preliminary study of the relationship between interannual and intraseasonal variability using 17 years (1979-1995) of European Centre for Medium-Range Weather Forecasts (ECMWF) and National Centers for Environmental Prediction/National Center for Atmospheric Research (NCEP/NCAR) reanalyses. They showed that, unlike the results from earlier model studies, there was not a common dominant mode which described monsoon variability on interannual and intraseasonal timescales. Also, their results suggested some influence of the boundary forcing, in this case ENSO, on the intraseasonal behaviour

of the monsoon. However, the sample size, encompassing only 2-3 El Niño/La Niña events, limited the statistical significance of the results. With the availability of the extended 40-year NCEP/NCAR reanalysis it is now possible to conduct a more extensive and statistically significant investigation into the relationship between monsoon subseasonal and interannual variability from which conclusions can be drawn regarding the prospects for dynamical seasonal prediction of the ASM.

2. The Data

The NCEP/NCAR Reanalysis is a joint project between NCEP and NCAR to produce a multi-decadal record of global atmospheric analyses with a data assimilation system that is unchanged (Kalnay et al. 1996). The data assimilation and forecast model are based on the global system that was implemented operationally at NCEP in January 1995. The model is run at a horizontal resolution of T62 and with 28 vertical levels. Moist convection is represented by a simplified form of the Arakawa-Schubert parametrization scheme (Pan and Wu 1994) and clouds are diagnosed from model variables using a scheme based on Slingo (1987). The NCEP model uses a 3-layer soil scheme based on that of Pan and Mahrt (1987) in which the temperature of the bottom layer is set to the annual mean climatological value.

Data were assimilated using a spectral statistical interpolation/3-D variational analysis method which requires no nonlinear normal mode initialization. Monthly mean upper air data on standard pressure surfaces have been supplied, already gridded on to a 2.5° latitude/longitude grid. Surface and 24 hour forecast fields (e.g., precipitation) are given on the equivalent T62 Gaussian grid. The spin-up of the hydrological cycle is small in the NCEP/NCAR reanalysis (e.g. Mo and Higgins 1996; Stendel and Arpe 1997).

For validating the subseasonal variations of rainfall from the reanalysis we compare with the Climate Prediction Center Merged Analysis of Precipitation (CMAP). This data set uses essentially the same algorithm and data sources as the monthly CMAP dataset described by Xie and Arkin (1997). The version we use is based on a blend of gauge data with satellite products, including GPI (GOES Precipitation Index based on geostationary infrared data), MSU (Microwave Sounding Unit), OPI (Outgoing longwave radiation-based Precipitation Index), SSM/I (Special Sensor Microwave/Imager) scattering and SSM/I emission. A detailed description of the pentad CMAP data set is in preparation (Pingping Xie, personal communication 1999).

3. Climatology and Interannual Variability

   a) 850hPa wind and precipitation

   One of the most dramatic elements of the summer monsoon is the development of the lower tropospheric Somali Jet in response to the land/sea gradient of large-scale heating. During the onset of the monsoon, in late May/early June, the gradient is mainly due to the land/sea temperature contrast associated with solar heating. As the monsoon develops, latent heating associated with convection plays an increasingly important role in the maintenance and evolution of the monsoon. The seasonal mean (June-September) 1958-97 climatologies of the 850hPa flow and rainfall are given in Figs. 1a and 1b. Orographic rainfall along the west coast of India is apparent, with a rainshadow effect to the east occurring due to the western Ghats. The monsoon trough exerts its primary influence on the rainfall over northeast India and the Bay of Bengal. Over China the monsoon flow is manifested as southerlies, and the TCZ extends into the western Pacific. These 40-year climatologies correspond closely to the 1979-95 climatologies presented in Annamalai et al. (1999). We find that compared to the Xie and Arkin (1996) observed rainfall the NCEP/NCAR precipitation is overestimated over China and the western tropical Indian Ocean, while it is underestimated over the western Pacific and near the equator in the central/eastern Indian Ocean. These shortcomings in the forecast rainfall have also been noted by Stendel and Arpe (1997) and Trenberth and Guillemot (1998). Thus, the NCEP/NCAR climatologies and their systematic errors of the ASM 850hPa flow and rainfall are robust for the 40-year record compared to the period 1979-95 when satellite data were incorporated into the reanalysis.

   Interannual variations of the summer monsoon system have been linked to ENSO boundary forcing (see Webster et al. 1998 for a review). The seasonal mean (June-September) standardized NINO3 SST anomalies for 1958-97 are given in Fig. 2a. During this period 10 El Niño and 10 La Niña events are in evidence based upon threshold cutoffs of +/-0.5 standard deviations. In the summer of 1997 the strongest NINO3 SST anomalies occurred as the 1997/98 El Niño event approached its mature phase. Analogously, the most negative NINO3 departure occurred during the development of the 1988/89 La Niña event.

   Two popular measures of monsoon variability are also given in Fig. 2. The AIR, constructed from a weighted average of 306 stations spread over the whole of the Indian subcontinent (Parthasarathy et al. 1994), is given in Fig. 2b. As discussed in Annamalai et al. (1999), when available in situ rainfall measurements should be used due to uncertainties in satellite derived rainfall estimates. It has long been
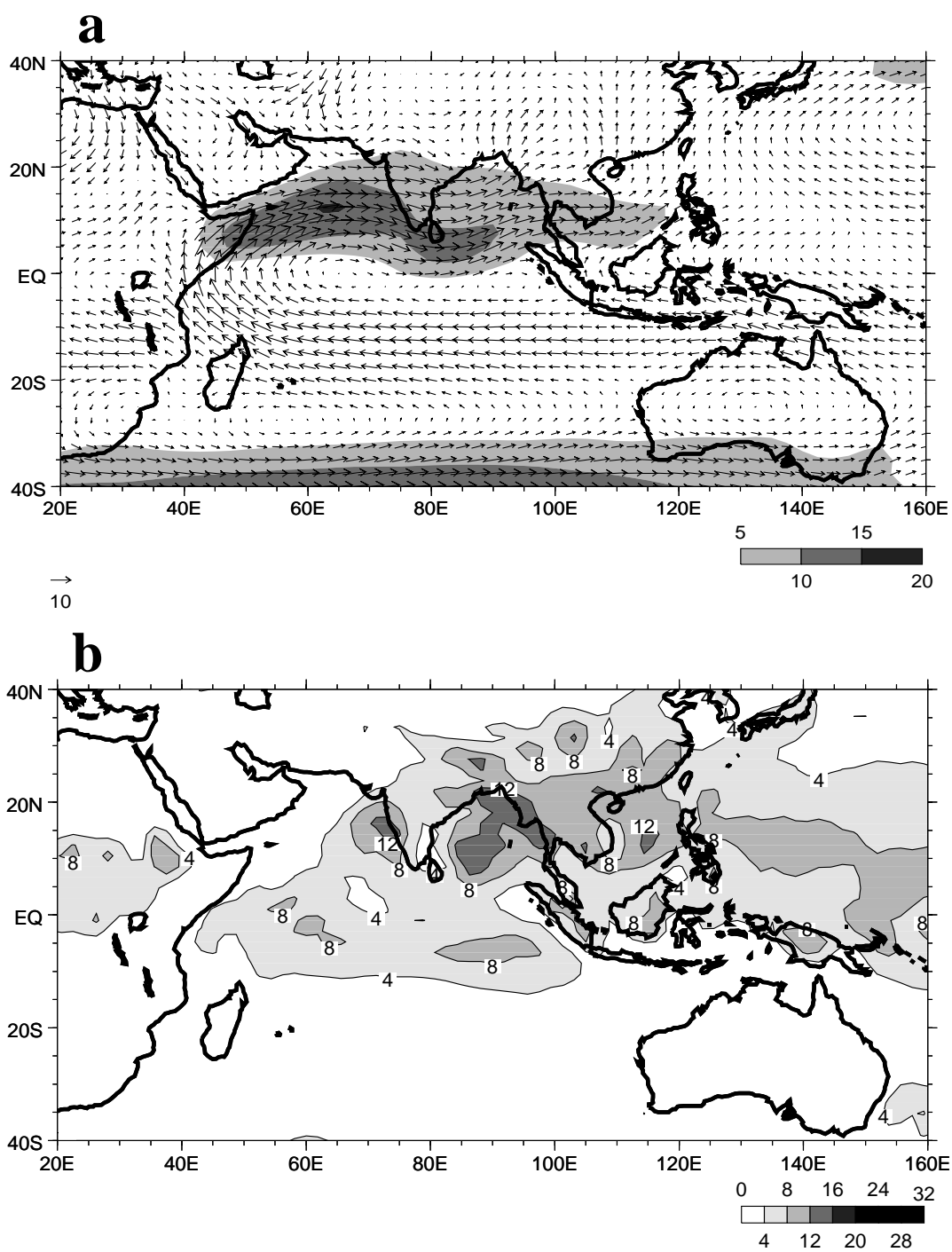
a

b

Figure 1: NCEP/NCAR reanalysis climatologies (1958-97) of the seasonal mean (June-September) (a) 850hPa wind (ms^{-1}), (b) rainfall (mm day^{-1}).

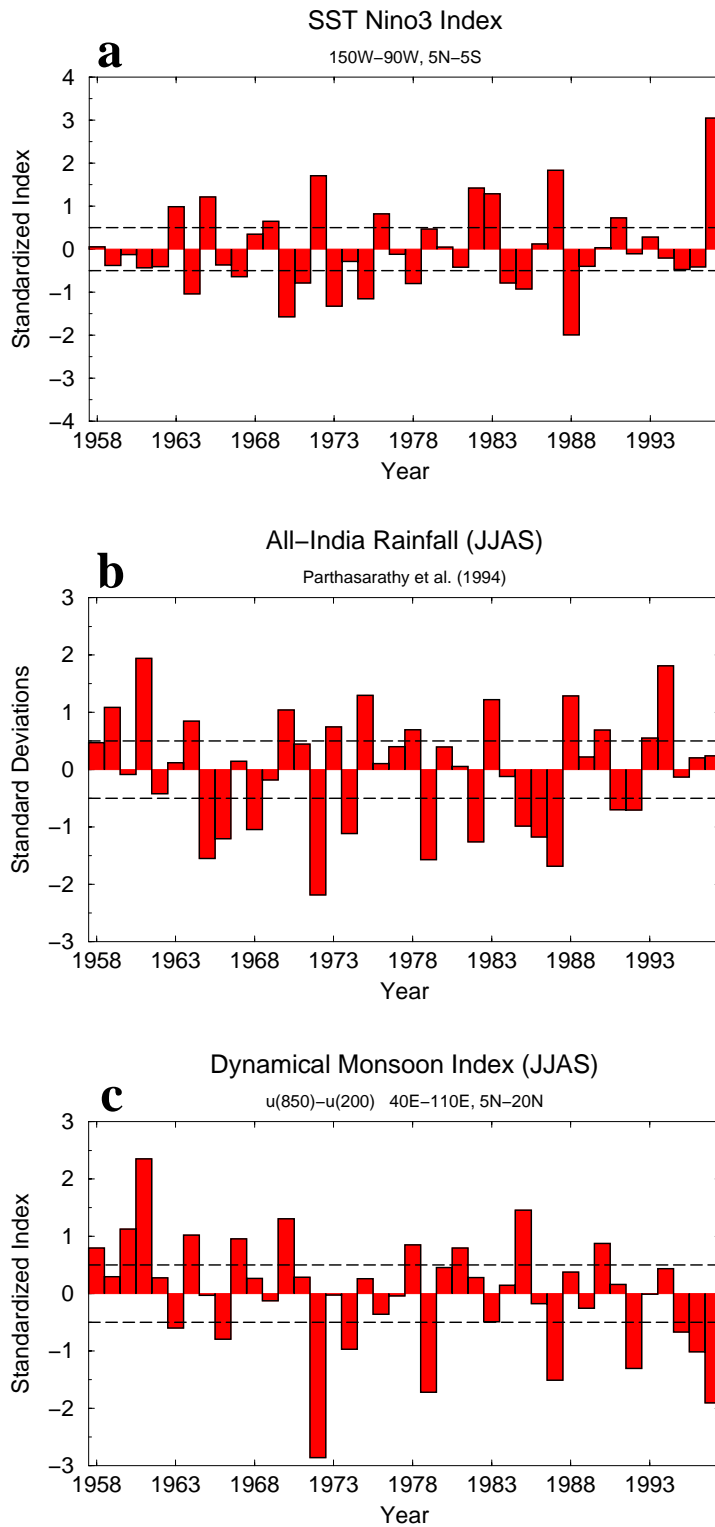Figure 2: Seasonal mean (June-September) indexes of (a) NINO3 sea surface temperature, (b) all-India rainfall, and (c) dynamical monsoon index. The indexes have been standardized by removal of the time mean and then dividing by the standard deviation of the interannual variability. Also plotted on each panel are the -0.5 and 0.5 standard deviation thresholds used for determining years of extreme variability.

known that Indian monsoon rainfall is related to Southern Oscillation (Walker and Bliss 1932), and ENSO in general. For the period of analysis the correlation between AIR and NINO3 SST is -0.46 consistent with the tendency for below (above) normal rainfall during El Niño (La Niña). A notable exception occurred during the summer 1997, when the strongest El Niño conditions in the record were manifested in the tropical Pacific Ocean, but the AIR was near normal. This clearly indicates the complexity of the summer monsoon system in that the SST variability in the tropical Pacific is but one of many possible modulators of summer monsoon variability.

The dynamical monsoon index (DMI), is a measure of the monsoon strength in terms of the zonal wind shear between 850hPa and 200hPa for the region 40°E-110°E, 5°N-20°N (Webster and Yang 1992). As seen in Fig. 2c, the DMI is characterized by strong interannual variations, as well as an interdecadal trend of decreasing wind shear. The DMI is a measure of the large-scale monsoon circulation, and hence does not necessarily correspond to the regional rainfall variations represented by AIR (Ju and Slingo 1995). For example, in 1983 and 1985 the strength of the monsoon implied by the DMI is opposite to that implied by the AIR, and this is reflected in the correlation of 0.56 between DMI and AIR. More importantly, Annamalai et al. (1999) demonstrated that DMI and AIR represent very different aspects of the spatio-temporal variability of the ASM.

Annamalai et al. (1999) noted that measures of weak/strong monsoon based on indices from reanalysis (e.g., DMI) are problematic. Instead they proposed that whenever possible the consistently measured AIR should be used to define weak/strong monsoon years over India. Associated with the interannual variations of AIR is a characteristic wind pattern at 850hPa. The wind anomalies in Fig. 3a have been constructed from the difference of the composites based on years of above normal versus below normal AIR using the +/-0.5 standard deviations thresholds given in Fig. 2b. This composite difference is nearly identical to the composite for 1979-95 (Annamalai et al. 1999), when the reanalysis is believed to be more reliable due to the incorporation of satellite data in the assimilation, thus indicating the robustness of this pattern of anomalies throughout the 40-year reanalysis. The composite difference of rainfall from the reanalysis is shown in Fig. 3b. The enhanced rainfall over India is consistent with the presence of cyclonic anomalies over the subcontinent, while the below normal rainfall to the south and west of India corresponds nicely to the anticyclonic anomalies. Additionally, negative rainfall anomalies and anticyclonic circulation is located in the foothills of the Himalayas near 90°E, 30°N. This interannual signal in the reanalysis precipitation has been confirmed since this pat-
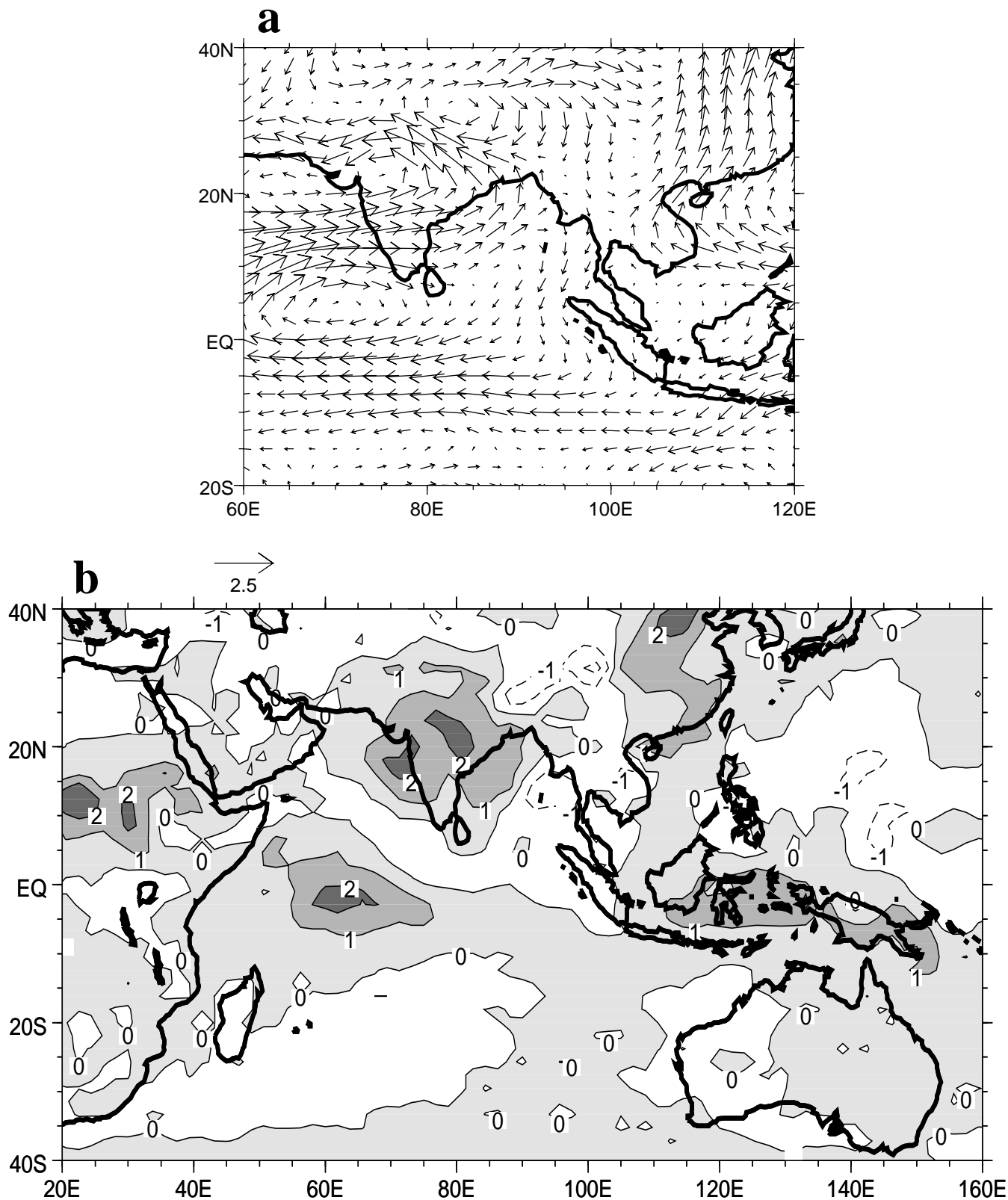
Figure 3: Difference of seasonal mean (June-September) composites of (a) 850hPa wind and (b) rainfall (mm day^{-1}) based on strong-weak years of all-India rainfall in Fig. 2b using 0.5 and -0.5 standard deviation thresholds to define extreme years.

tern agrees well with that obtained for the period 1979-95 (Annamalai et al. 1999, their Fig. 9e) from compositing the observed rainfall estimates of Xie and Arkin (1996). Additionally, these results are consistent with the finding of Sikka (1980) with respect to years of "good" and "bad" monsoon rainfall where "The differences are most marked in the region of the monsoon trough (20-25⁰N), viz., the anomalous winds [at 700hPa] are markedly cyclonic in the case of [the] good monsoon composite."

b) Dominant modes of interannual variability

For investigating the relationship between subseasonal and interannual variability we concentrate on the 850hPa flow over the region 60°E-120°E, 20°S-40°N, the same region analyzed by Annamalai et al. (1999). The domain was not extended further east to exclude contaminating the analysis by the direct effects of ENSO. The 850hPa flow is an excellent candidate for investigating the interannual (and subseasonal) variability of the ASM since it captures aspects of both the large-scale and regional-scale flow.

The first empirical orthogonal function (EOF-1) and principal component (PC-1) of the seasonal mean (June-September) wind anomalies (relative to the 40-year climatology) are presented in Figs. 4a and 4b respectively. EOF-1 is dominated by near-equatorial easterly anomalies, while the westerly anomalies further north (10°N-20°N) and southerlies over China correspond to stronger than usual monsoon circulation during the early portion of the record when PC-1 is positive (Fig. 4b). During the latter portion of the record PC-1 is dominated by negative values, indicating a reversal of the anomalous flow.

The composite difference of rainfall from the reanalysis for strong-weak years based upon +/-0.5 standard deviation cutoffs of PC-1 is shown in Fig 4c. There is a north/south dipole of rainfall anomalies in which enhanced precipitation over the continental latitudes of the ASM is associated with a stronger monsoon flow, while further south near 5°N there is below normal precipitation. Also seen in the rainfall composite difference is the strong signal over Africa that is consistent with the decadal modulation of Sahel and Sudan rainfall (Rowell et al. 1995). This suggests that the trend in PC-1 may be physically realistic.

The trend of weakening westerly anomalies from 10°N-20°N is consistent with the trend of weaker DMI seen in Fig. 2c. To further explore the possibility that the trends in PC-1 and the DMI are real, and potentially linked to the boundary forcing, we have performed an EOF analysis of seasonal mean (June-September) observed
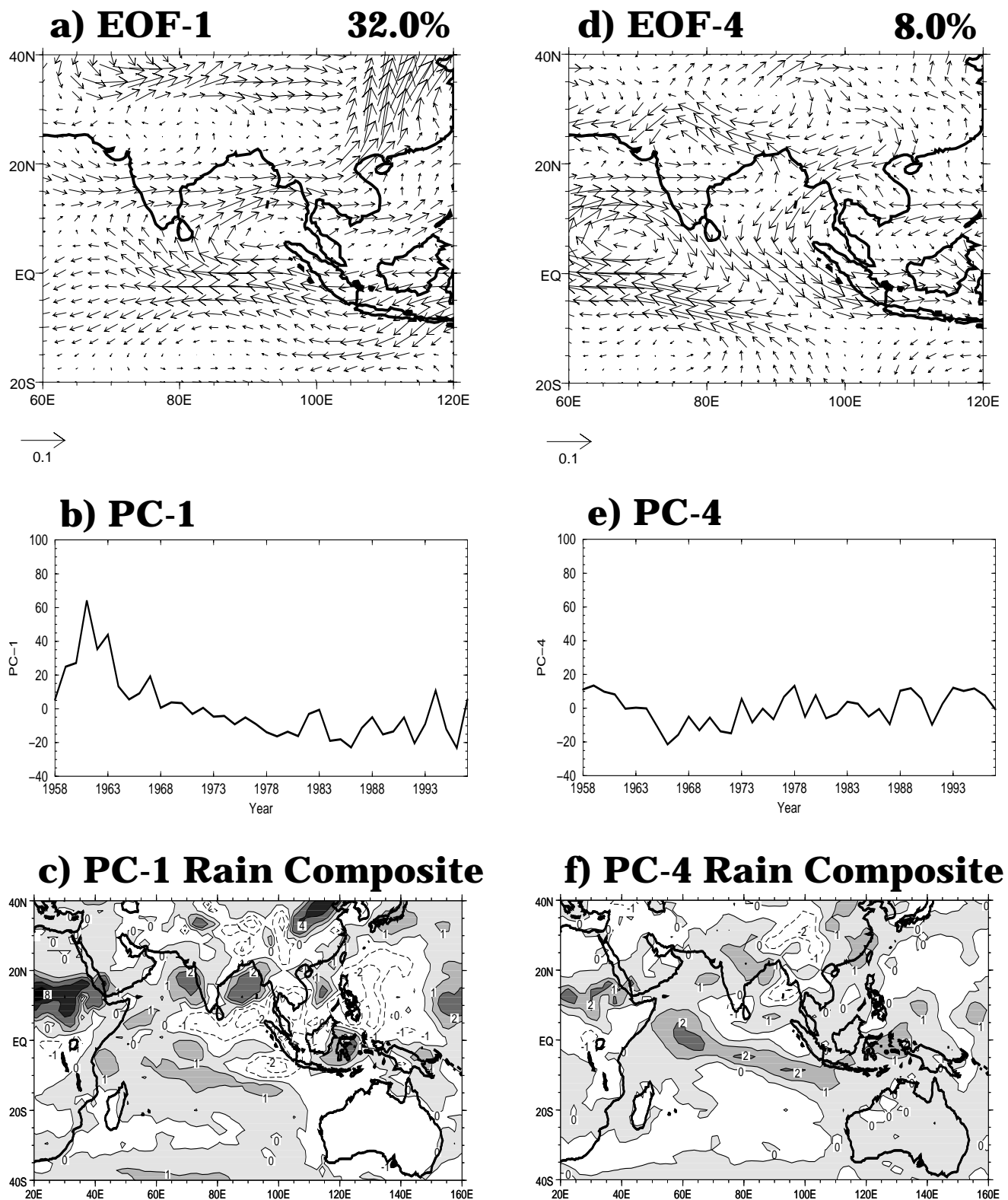
Figure 4: Results of an empirical orthogonal function (EOF) analysis of NCEP/NCAR seasonal mean (June-September) 850hPa wind anomalies for 1958-97. (a) EOF-1, (b) PC-1, (c) difference of seasonal mean (June-September) composites of rainfall (mm day^{-1}) for strong-weak years of PC-1 using 0.5 and -0.5 standard deviation thresholds of PC-1 in (b), (d) EOF-4, (e) PC-4, (f) as (c) but for PC-4 in (e). The percent variance explained by each mode is also given.

SST and reanalyzed ground temperature anomalies over land for the monsoon domain. As seen in Fig. 5a, the leading mode explains ~30% of the total interannual variability, having positive loadings over the vast majority of the domain, with PC-1 (Fig. 5b) being dominated by a warming of approximately 0.5^oK over the period 1958-97. Closer scrutiny indicates that the spatial loadings over land, especially east of 80^oE, are smaller than those over the near-equatorial Indian Ocean. This indicates a reduction in the land/sea temperature contrast during the latter portion of the record, consistent with the weaker DMI and weaker westerlies from 10^oN-20^oN and the weaker monsoon southerlies over China. The DMI and PC-1 of the surface temperature have a correlation of -0.41, significant at the 5% level. It will be of interest to evaluate the robustness of the trends in the low-level flow and the DMI using the 40-year European Centre for Medium-Range Weather Forecasts Reanalysis, when it becomes available.

Since the dominant mode of interannual variability in the 40-year record is influenced by decadal and longer trends in monsoon strength, no direct counterpart to the dominant interannual modes from the 1979-95 period as documented in Annamalai et al. (1999) has been found, although EOFs 2 and 3 contain elements of these modes. However, examination of the higher order modes revealed that EOF-4 (Fig. 4d) has a very similar pattern to that obtained by compositing on AIR (Fig. 3a), particularly in the vicinity of India. Similarly, the composite difference of rainfall (Fig. 4f) associated with PC-4 (Fig. 4e) corresponds closely to that based on AIR (Fig. 3b). Importantly, the principal component time series of EOF-4 (Fig. 4e) has a correlation of 0.60 (significant at 1% level) with respect to the observed AIR (Fig. 2b). Thus, the similarity of the spatial patterns of EOF-4 and its associated rainfall anomalies (Figs. 4d, f) with that of the composites based on AIR (Fig. 3), plus the high temporal correlation of PC-4 with observed AIR provides confirmatory evidence that the EOF analysis has extracted a physically realistic mode of summer monsoon variability.

4. Subseasonal variability

    a) Dominant modes

EOF analysis of the daily 850hPa flow for JJAS 1958-97 is performed for the same domain used for the study of interannual variability (60^oE-120^oE, 20^oS-40^oN). Prior to the EOF analysis we remove at each gridpoint the climatological daily means based upon the 40 summers of data. The first four EOF's are shown in Fig. 6. EOF-1 (Fig. 6a), explaining 13% of the total variance, is dominated by intraseasonal timescales with the dominant power occurring between 40-60 days, and a secondary
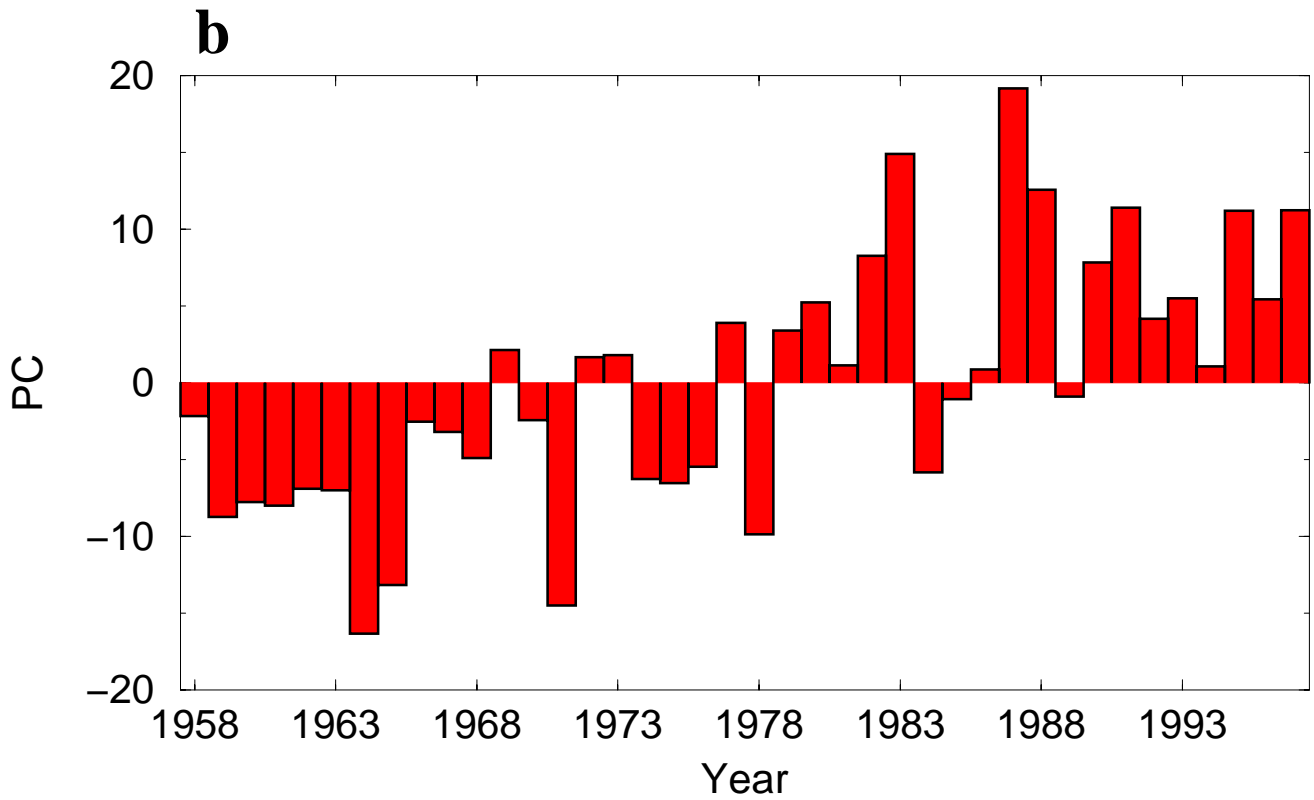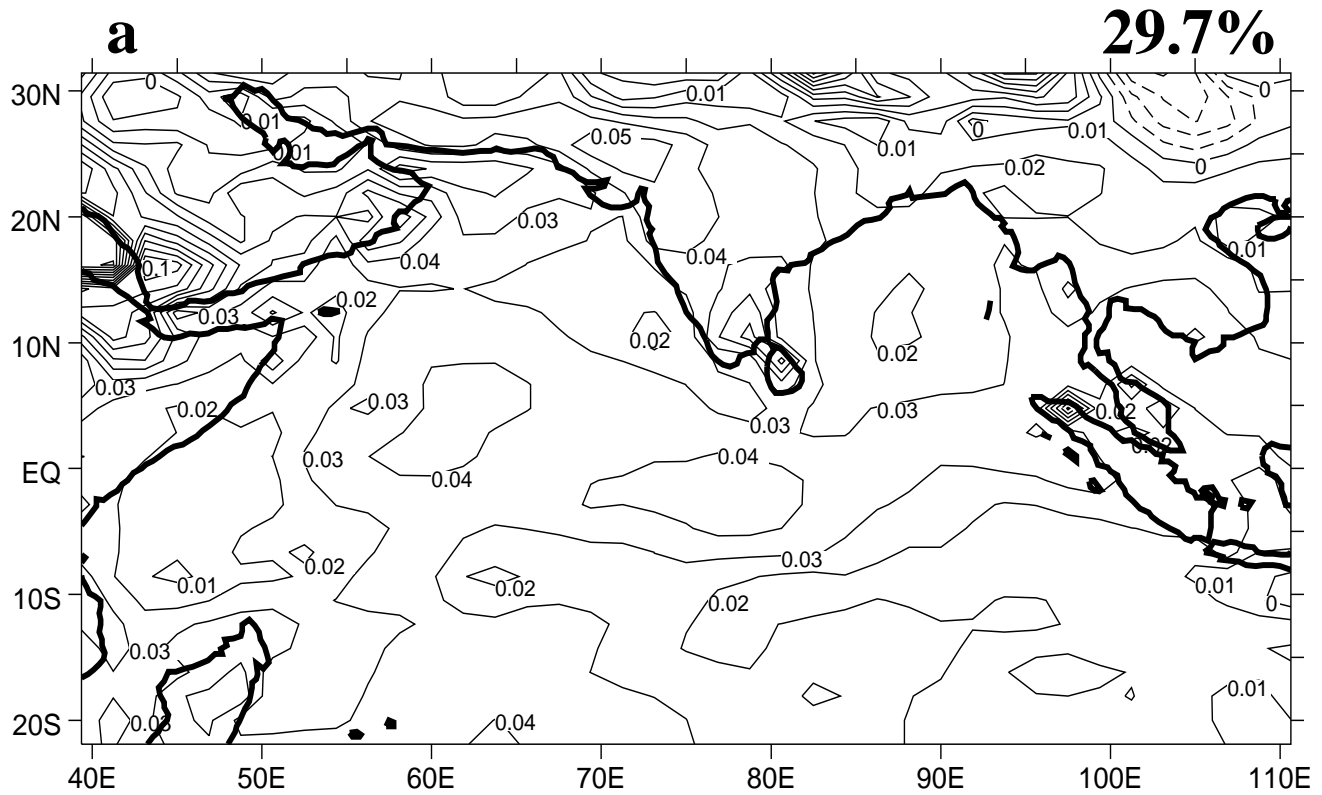
Figure 5: Results of an EOF analysis of seasonal mean (June-September) anomalies of observed sea-surface temperature and reanalyzed ground temperature over land for 1958-97. (a) EOF-1, (b) PC-1. Over the 40-year period this corresponds to a warming of approximately 0.5°K. The percent variance explained is also given.

peak near 17 days (Fig. 7a). The spatial pattern of this mode is consistent with the boreal summer 30-60 day mode that Goswami et al. (1998) identified in NCEP/ NCAR surface winds for 1987-96 based on composite analysis. EOF-2 and EOF-4 have similar spatial structures relative to EOF-1, and they are also dominated by timescales of ≥30 days (Figs. 7b and 7d). Further scrutiny reveals that together these 3 modes represent various stages in the life cycle of northward propagating intraseasonal variations of the TCZ, describing one aspect of the active and break cycle of the ASM. The rainfall anomalies associated with these modes are given in Figs. 8a, b, and d. These are composite differences of precipitation for +/-1 standard deviation thresholds of the respective PC's. For these 3 modes, the tendency is for enhanced rainfall to occur in conjunction with the westerly anomalies and the cyclonic flow evident to their north, while south of the westerlies the rainfall tends to be below normal thus reflecting a north/south dipole of convection. These three modes characterize the preferred locations of the TCZ, over the land during the active phase (EOF-2 and EOF-1). During the active phase the extension of the convective zone from India into the western Pacific is consistent with the intraseasonal cloudiness variations analyzed by Yasunari (1979) and the NOAA satellite imagery presented in Sikka and Gadgil (1980). Where the EOF-1 related rainfall perturbations are strongest, in the eastern tropical Indian Ocean, the South China Sea and the western Pacific, is the location of the main axis of convection and the maximum variance of boreal summer OLR on timescales of 25-70 days given by Vincent et al. (1998). EOF-4 (Fig. 6d) is characteristic of break conditions of the monsoon, with the enhanced precipitation being located in the foothills of the Himalayas (Fig. 8d), while further south over India and southeast Asia below normal rainfall is present, consistent with the break conditions characterized by Ramanadham et al. (1973).

The composite rainfall anomalies (from the reanalysis) associated with these modes of variability, shown in Fig. 8, can be validated against composites obtained from the pentad Climate Prediction Center Merged Analysis of Precipitation (CMAP, Xie and Arkin 1999, in preparation) for the period 1979-95 (Fig. 9). This validation is possible since the modes presented in Fig. 6 are very robust, being virtually identical to those obtained from a separate EOF analysis of daily data for JJAS 1979-95 (not shown). Relative to the CMAP composites, the reanalysis composites capture well the band of enhanced rainfall associated with the TCZ and its northward propagation defined by EOF-1, EOF-2 and EOF-4. However, for modes 1 and 2 the rainfall anomalies in the equatorial Indian Ocean in the CMAP data are not properly represented by the reanalysis. As noted by Annamalai et al. (1999), and seen in Fig. 1b,

a) EOF-1 **13.0%**

b) EOF-2 **7.6%**

c) EOF-3 **6.6%**

d) EOF-4 **4.9%**
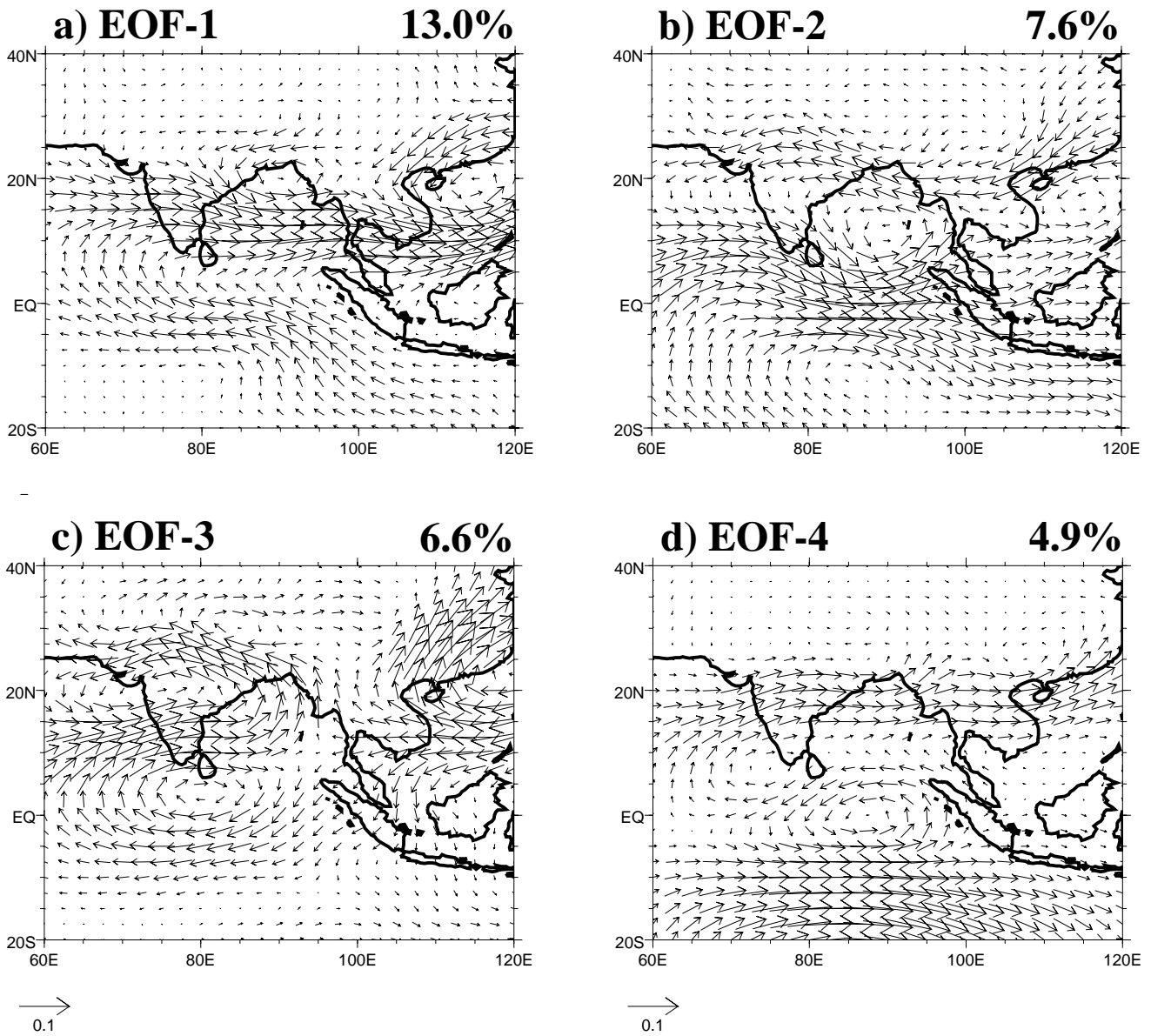
Figure 6: Results of an EOF analysis of NCEP/NCAR daily 850hPa wind anomalies for June-September 1958-97. Prior to the analysis the climatological daily means have been removed. (a) EOF-1, (b) EOF-2, (c) EOF-3, (d) EOF-4.
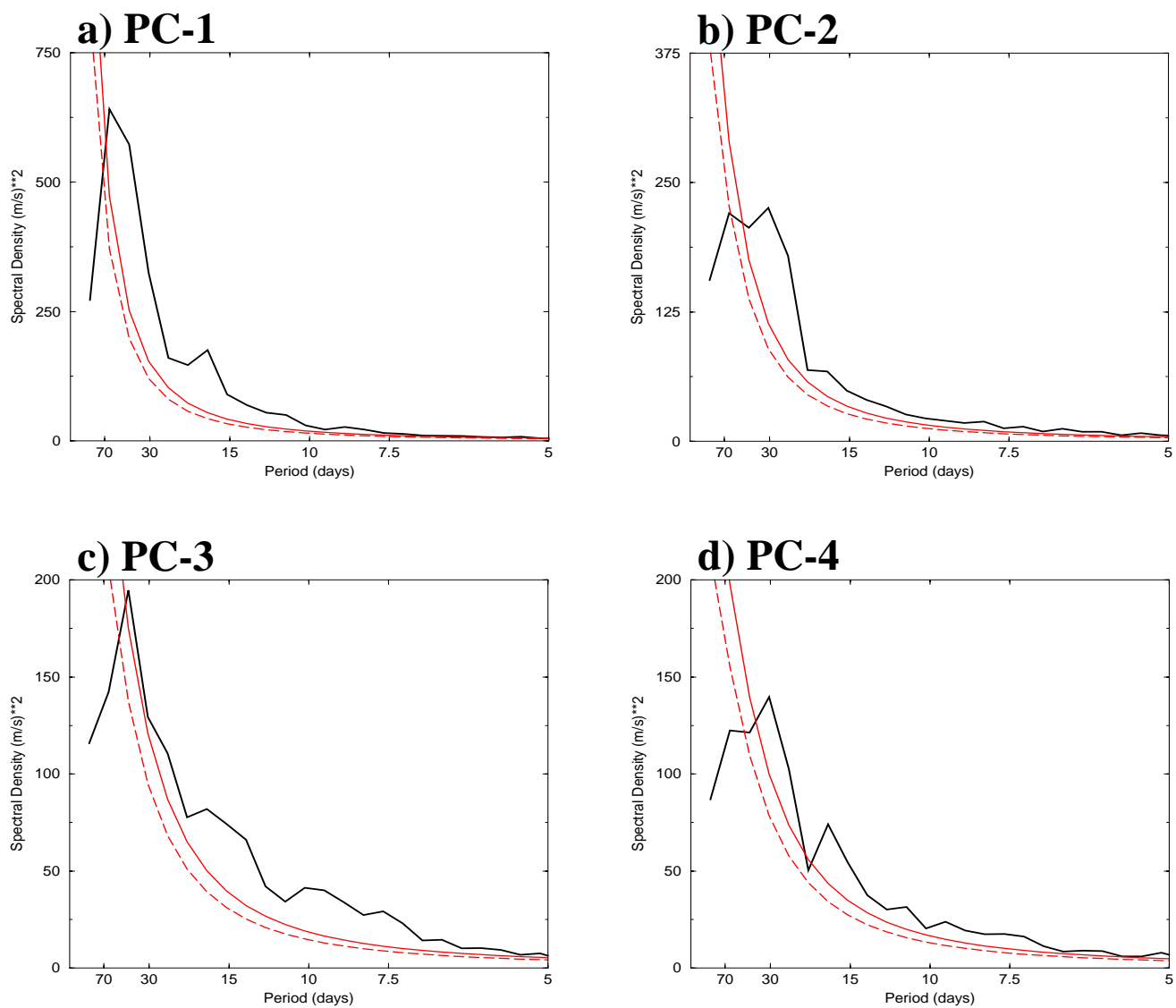
Figure 7: Power spectra of the principal component time series of EOF's 1-4 given in Fig. 6. Also shown are the null and 95% confidence rednoise levels (dashed and solid light-shaded lines). These are the averages of the power spectra from each summer.

Figure 8: Difference of daily composites of NCEP/NCAR rainfall (mm day^{-1}) based on strong -weak days of the principal components time series of EOF's 1-4 given in Fig. 6 using 1.0 and -1.0 standard deviation thresholds to define extreme days.
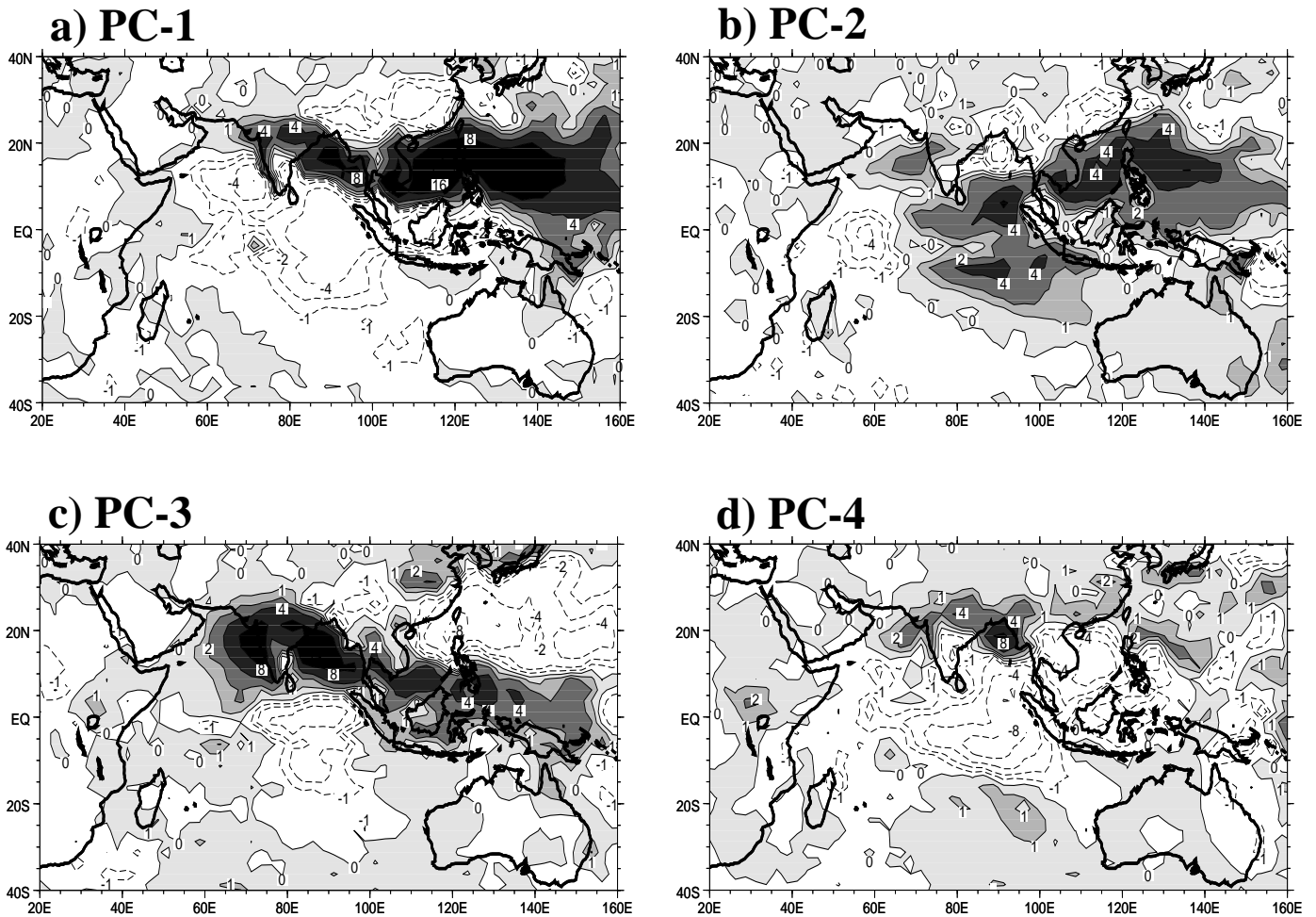
Figure 9: Difference of pentad composites of the observed Climate Prediction Center Merged Analysis of Precipitation (CMAP) rainfall (mm day^{-1}) based on strong-weak pentads of the pr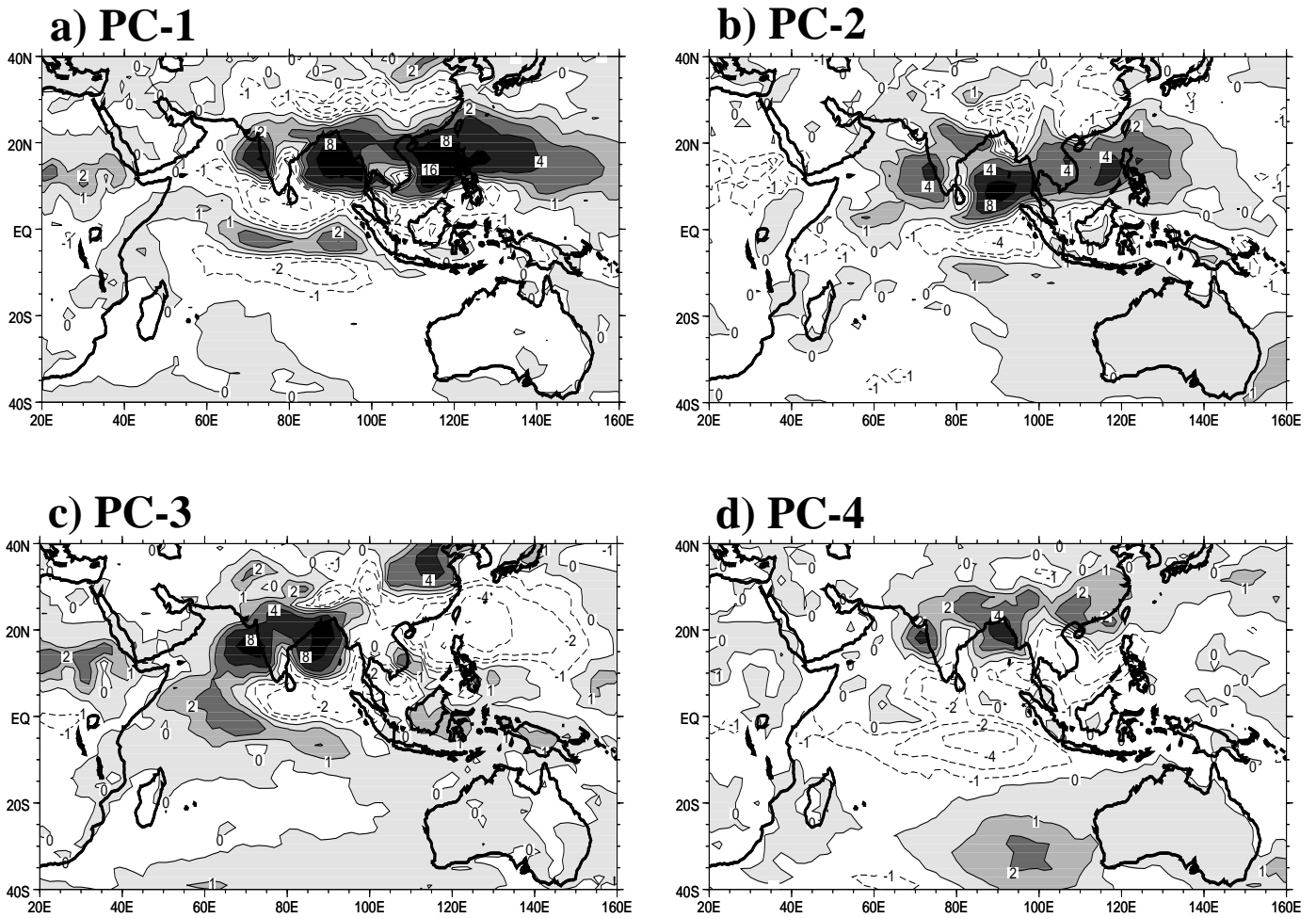incipal components time series of EOF's 1-4 obtained from an EOF analysis of NCEP/NCAR daily 850hPa wind anomalies for June-September 1979-95. The daily principal component time series were standardized and then pentad averaged with extreme pentads defined using 1.0 and -1.0 standard deviation thresholds. The EOF's (and PC's) obtained from the analysis of June-September 1979-95 are virtually identical to those given in Fig. 6 for June-September 1958-97. Thus we employ this subset of observationally based rainfall composites as validation of the NCEP/NCAR rainfall presented in Fig. 8.

the reanalysis rainfall is problematic in the equatorial Indian Ocean. Even given this shortcoming over the equatorial Indian Ocean, the reanalysis captures realistically the northward propagation of the TCZ associated with active/break cycles of the ASM on intraseasonal timescales.

A main tenet of the hypothesis that perturbations to subseasonal variability control the interannual variability is that the patterns of subseasonal and interannual variability should correspond (Palmer 1994). We have found that the third mode of subseasonal variability (EOF-3, Fig. 6c) exhibits the anticyclonic/cyclonic/anticyclonic pattern in the vicinity of India that characterizes the interannual wind anomalies (Fig. 3a and Fig. 4d), although the oceanic anticyclone is located directly south of India in the daily analysis. Time series analysis of the PC-3 time series indicates this mode of variability to be dominated by periods of 7-40 days (Fig. 7c), the timescales that are considered important for active/break periods of rainfall over India. As seen in Fig. 8c, the composite rainfall difference indicates enhanced rainfall in the vicinity of the Indian subcontinent when cyclonic anomalies prevail over this region. Similarly, enhanced rainfall occurs in the vicinity of the Maritime continent where the flow also has a cyclonic tendency. Where the flow is anticyclonic (south of India and near the South China Sea) negative rainfall anomalies occur in the composite rainfall difference pattern. This quadrupole pattern of rainfall anomalies is manifested as a southeastward tilt of enhanced rainfall, extending from India into the equatorial western Pacific. This southeastward tilt is readily apparent in the CMAP validation data (Fig. 9c), indicating that the reanalysis does not properly capture the enhanced rainfall in the vicinity of Malaysia. Even so, the reanalysis rainfall composite difference captures the main elements of the well documented pattern associated with active (wet) versus break (dry) phases of the summer monsoon over India (Ramamurthy 1969). The patterns of rainfall and 850hPa wind anomalies are consistent with the composites presented by Webster et al. (1998) that were generated with respect to the active and break periods of Indian monsoon. Additionally, these convective anomalies are consistent with an analysis of cloudiness by Murakami (1976) and the one-point correlations of precipitation with extended Indian monsoon rainfall (Goswami et al. 1999). Also, the southeastward tilt of enhanced rainfall corresponds to the "axes of minimum OLR" and maximum variance of OLR on 6-25 day timescales given by Vincent et al. (1998). The northward propagation of this convective quadrupole was captured in the extended EOF analysis of OLR by Lau and Chan (1986, their Fig. 9), and the importance of this mode of variability for the Indian monsoon region was underscored by Wang and Rui (1990, their Fig. 6) who presented an excellent example of

the northward propagation of this quadrupole pattern of convective anomalies from late in the summer monsoon season of 1984 using OLR.

Analysis of the daily data has revealed the presence of two main types of convective phenomenologies over the ASM region. The first, described by EOF's 1, 2, and 4, characterizes the low-frequency (intraseasonal) northward propagations of the TCZ. This is a large-scale phenomenon that is zonally oriented, describing the north/south dipole of the continental and oceanic convective regimes. The convective anomalies are most pronounced over the South China Sea and the west Pacific, with a weaker signal over the Bay of Bengal and India. The second regime is described by EOF-3. The main centers of action consist of a quadrupole pattern in the 850hPa winds, with anticyclonic flow to the south of the India and cyclonic flow over the bulk of the subcontinent. East of 95°E the anomalies are reversed, thus there is a pronounced southeastward tilt to the rainfall anomalies, with the dominant impact being located over India and the Bay of Bengal. A benefit of the long record of NCEP/NCAR reanalysis is the isolation of these two regimes of subseasonal variability. As cited above, various authors have detected the southeastward tilt of convection (e.g., Murakami 1976), while others found the TCZ to be more zonal (e.g., Yasunari 1979), leading Gadgil and Asha (1992) to speculate that this "may be due to difference(s) in the quality of the data over the two periods," which is not the case based on our analysis.

Importantly, the subseasonal wind and rainfall anomalies associated with EOF-3 Figs. 6c, 8c, 9c) exhibit nearly identical patterns as found on interannual timescales (Fig. 3, and Figs. 4d-f). This result suggests the viability of a link between subseasonal and interannual variability, and supports the hypothesis of Palmer (1994) and Fennessy and Shukla (1994) that there is a common mode of variability for the Indian summer monsoon.

b) The relationship between Subseasonal and Interannual Variability

Closure of the link between subseasonal and interannual variability is established by demonstrating that a subseasonal mode projects on to the interannual variability, or by establishing that a mode is influenced by interannual variations of the boundary forcing. In the case of AIR, the afore-mentioned results suggest that EOF-3/PC-3 is a mode through which the subseasonal and interannual variations are related. It is therefore of interest to establish the importance of this mode for high frequency variations of AIR. As seen in Fig. 10, 1987, a period studied intensively by the Monsoon Numerical Experimentation Group (MONEG; WCRP 1992, 1993), is an illustrative example of the importance of PC-3 for variations of daily AIR, particularly
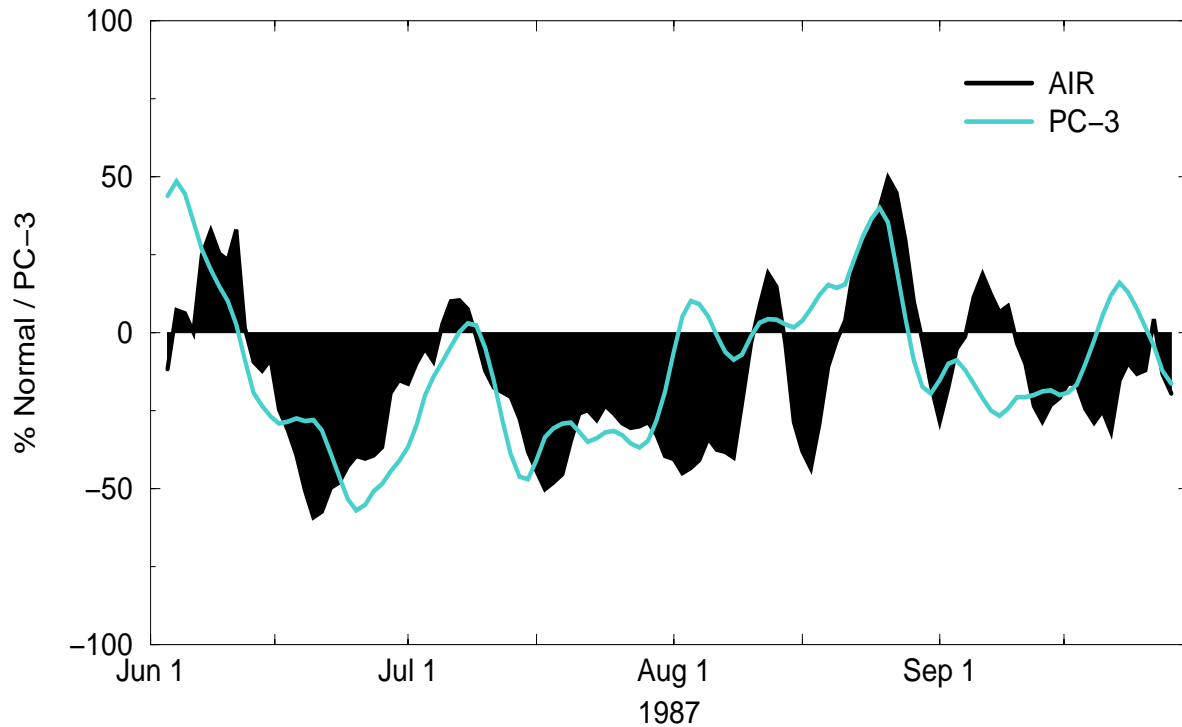
Figure 10: For 1987 the observed (filled black curve) daily all-India rainfall (expressed as departures from normal) are compared with PC-3 (light-shaded line) of EOF-3 in Fig. 6c. The data have been smoothed with a 5-day running mean. For all-India rainfall the departures from normal are calculated relative to the climatological daily means for 1971-95.

during the months of June and July. As seen in Table 1, the correlation of these two time series is 0.59, significant at the 5% level (assuming 10 degrees of freedom or greater during the 122 day season). Table 1 clearly indicates that on subseasonal timescales the variations of AIR correspond most closely to the changes of the PC-3 time series. With few exceptions (1973, 1985, 1988 and 1990), the correlations of the other PCs' with the daily AIR are typically much smaller (or even negative). Our results unequivocally establish that subseasonal mode-3 is the principal modulator of the short-term variations of Indian summer monsoon rainfall.

It should be noted that 1987 was a year of below normal AIR, and this is clearly reflected in the bias of the PC and the AIR departures towards negative values during this summer (Fig. 10). The seasonal average of the daily principal component time series is an integrated measure of the influence of the subseasonal mode on the total seasonal anomaly. Calculating the seasonal average of PC-3 for each summer 1958-97 ($\overline{PC-3}$, Table 2), and correlating with observed seasonal mean anomalies of AIR (Fig. 2b) results in a correlation of 0.67 (significant at the 1% level), thus directly linking the interannual variations of observed AIR to the projection of subseasonal mode-3 onto interannual timescales. For $\overline{PC-1}$, $\overline{PC-2}$, and $\overline{PC-4}$ the correlations with AIR are much weaker, 0.23, -0.13, and 0.04 respectively, indicating that the projection of these subseasonal modes on to interannual variations of Indian monsoon rainfall is tenuous at best.

We can further illustrate the link between subseasonal and interannual timescales by examining the probability distribution functions (PDF's) of the principal component time series. In Fig. 11 we show the standardized PDF's of the daily PC's using all years of data (thick solid line), and for years of above normal AIR (thick long-dashed line) and below normal AIR (thin short-dashed line) as determined from Fig. 2b. As suggested by the negative bias of PC-3 in 1987 (Fig. 10), the probability distribution function of PC-3 (Fig. 11c) is systematically perturbed towards negative values during years of below normal AIR, whereas it is perturbed towards positive values during years of above normal AIR. The changes in the means of the PDF's are significant at the 2.5% level (see the Appendix for a discussion of the t-test as employed herein). However, the forcing that causes the shift in the mean of the PDF has yet to be isolated. Thus, at the present time, probabilistic seasonal forecasts of Indian monsoon using this mode of variability are not possible. The PDF's of PC-1, PC-2 and PC-4 do not exhibit any systematic perturbations with respect to years of above-normal or below-normal AIR. This is consistent with their weak projection on to the daily variations of AIR (Table 1) and the poor correlations of the seasonal means of these

Table 1: Correlations of observed all-India rainfall for each summer (June-September) with the principal component timeseries associated with the EOF patterns in Fig. 6. Prior to calculating the correlations a 5-day running mean was applied to the data.

Year	PC-1	PC-2	PC-3	PC-4
1971	0.30	-0.13	0.70	0.60
1972	0.09	0.03	0.79	0.29
1973	0.35	0.26	0.36	0.45
1974	-0.18	0.24	0.52	0.02
1975	-0.22	0.02	0.69	0.26
1976	-0.23	-0.11	0.54	0.28
1977	-0.04	0.26	0.65	0.30
1978	0.06	0.14	0.54	0.03
1979	0.46	0.45	0.64	0.28
1980	-0.20	0.36	0.65	0.11
1981	-0.21	-0.06	0.42	0.22
1982	-0.01	-0.11	0.69	0.60
1983	-0.08	-0.27	0.64	0.54
1984	0.01	-0.23	0.44	0.05
1985	-0.45	-0.25	0.30	0.39
1986	0.12	0.39	0.64	0.57
1987	0.41	0.05	0.59	0.37
1988	0.20	0.51	0.16	0.19
1989	-0.12	0.01	0.64	0.59
1990	0.19	0.37	0.24	0.02
1991	-0.12	0.20	0.54	0.19
1992	0.36	0.29	0.66	0.19
1993	0.02	0.11	0.59	0.03
1994	0.28	0.48	0.64	0.02
1995	0.27	0.15	0.69	0.46

Table 2: Seasonal means (June-September) of the principal components of the daily 850hPa wind for 1958-97. The associated EOF patterns are presented in Fig. 6.

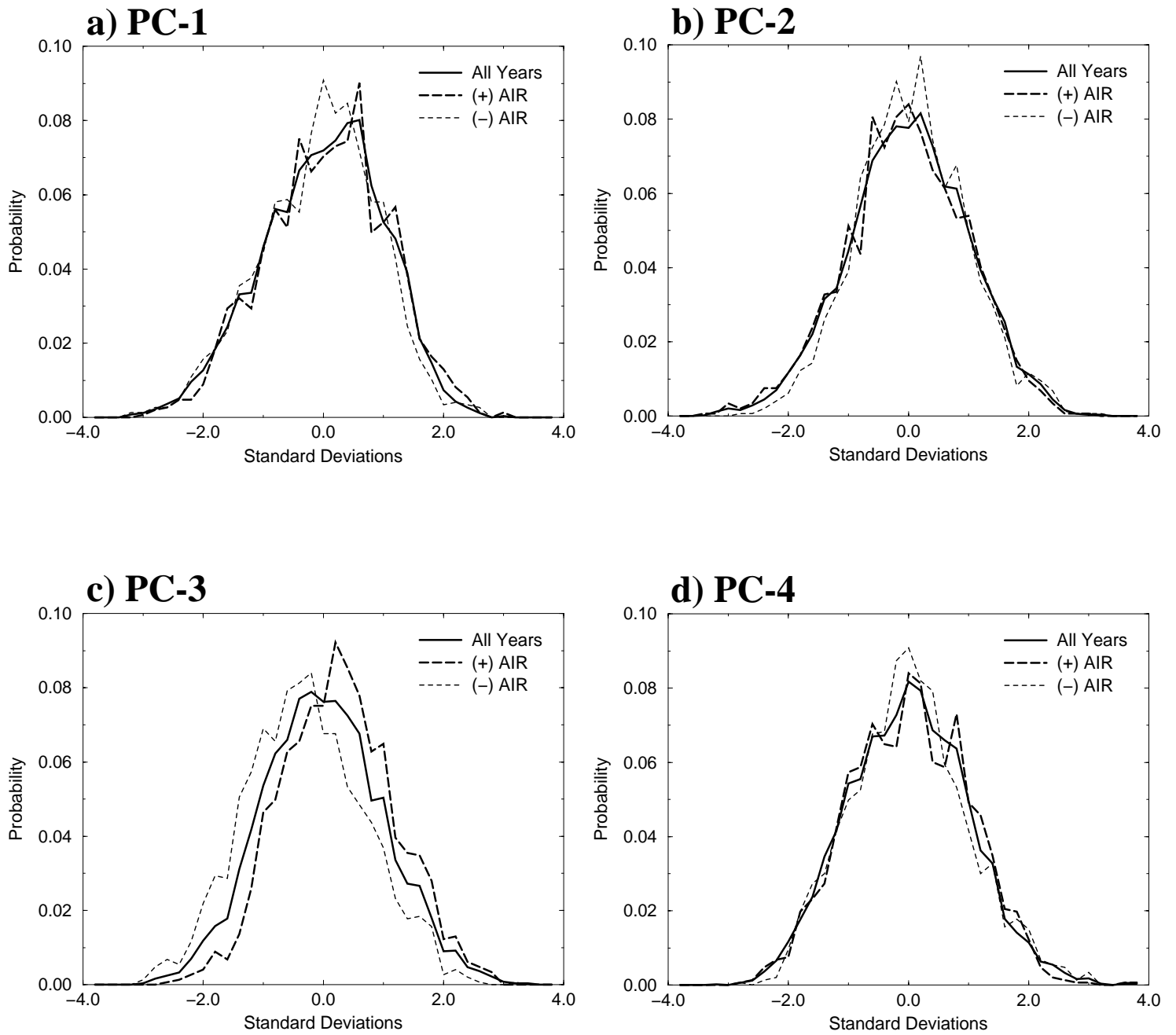| Year	PC-1	PC-2	PC-3	PC-4	Year	PC-1	PC-2	PC-3	PC-4
1958	1.4	7.2	10.3	1.5	1978	10.0	18.6	0.1	-1.4
1959	4.7	-8.8	21.0	-1.3	1979	-12.9	4.5	-8.5	-6.8
1960	5.4	-1.6	11.0	-3.5	1980	-2.9	12.7	5.6	-11.3
1961	38.5	-34.4	24.8	6.4	1981	-3.7	14.2	-8.4	6.5
1962	15.2	-19.2	12.1	-3.5	1982	10.3	-0.2	-8.4	-5.0
1963	17.8	-29.5	12.7	0.4	1983	-12.5	-7.4	11.7	-2.3
1964	-5.5	-4.6	10.4	-0.9	1984	-6.5	17.2	-8.3	7.5
1965	5.2	-5.9	-8.0	-1.2	1985	1.6	14.5	-19.6	2.6
1966	-9.9	-17.3	-2.7	-6.0	1986	-2.7	14.9	-11.5	3.3
1967	17.9	-9.2	0.2	-4.3	1987	-15.4	-7.2	-10.5	2.2
1968	8.4	5.5	-1.7	1.2	1988	-17.3	-9.6	7.1	-8.4
1969	-0.9	-3.9	-0.8	-4.9	1989	-7.9	6.6	-2.8	-4.1
1970	-2.3	4.0	5.2	-2.7	1990	6.5	14.2	-9.6	5.7
1971	-8.2	5.0	0.1	10.8	1991	3.3	-1.2	-7.9	7.9
1972	0.9	-4.2	-13.1	-1.3	1992	-10.7	14.2	-7.9	-3.9
1973	-5.5	11.8	7.7	7.3	1993	-3.2	-1.1	-0.6	-0.5
1974	-6.4	3.2	-2.4	13.6	1994	25.1	-9.7	2.3	-2.1
1975	-10.2	12.9	2.7	3.9	1995	-13.6	0.0	3.2	-14.2
1976	-2.8	2.3	-5.1	-0.1	1996	-22.5	9.7	-0.8	6.1
1977	1.0	3.3	-3.1	-3.9	1997	10.4	-21.8	-6.5	6.7

Figure 11: Probability distribution functions (PDF's) of the principal component time series of EOF's 1-4 given in Fig. 6. Each of the principal component time series were standardized prior to calculating the PDF. The solid line is the PDF based on all year of data. The thick dashed line is the PDF for years when the observed all-India rainfall was above normal (≥ 0.5 standard deviation in Fig. 2b), and the thin short dashed line is the PDF for years when the observed all-India rainfall was below normal (≤ -0.5 standard deviation in Fig. 2b).

$\overline{PC's}$ (Table 2) to interannual variations of AIR as noted in Table 1. That subseasonal PC-1 is not perturbed with respect to interannual variations of AIR is consistent with the result of Annamalai et al. (1999) in their analysis of NCEP/NCAR and European Centre for Medium-Range Weather Forecasts (ECMWF) Reanalyses for 1979-95. They concluded "On the regional scale of AIR, there does not appear to be such a relationship, at least in terms of the dominant mode of intraseasonal variability."

Our findings, and those of Annamalai et al. (1999), are not consistent with the result of Goswami et al. (1998), who analyzed 10 years of NCEP/NCAR reanalyzed surface winds. They concluded "the composite structure of the 30-60 day mode is strikingly similar to the dominant mode of interannual variability of the seasonal mean winds indicating a strong link between the intraseasonal oscillations and the seasonal mean." The interannual variability of the seasonal mean winds was the composite difference of strong versus weak years of AIR (their Fig. 17), which more closely resembles our composite difference (Fig. 3a) and our subseasonal EOF-3 (Fig. 6c) than it does their 30-60 day mode (which corresponds to our EOF-1, Fig. 6a). They used unfiltered daily relative vorticity over two regions, 70-100°E, 12-22°N and 70-100°E, 5°S-10°N, and assumed incorrectly that these variations were representative of the two preferred locations of the TCZ associated with the 30-60 day mode. By using unfiltered data they included all modes and timescales of subseasonal variability, with the afore-mentioned locations corresponding closely to the cyclonic/anticyclonic couplet near India in EOF-3 (Fig. 6c). Additionally, they computed the residence time of the TCZ based on the number of days that the positive (cyclonic) relative vorticity over 70-100°E, 12-22°N exceeded a critical value. They found that for 1987 (1988) a shorter (longer) residence time was associated with below (above) normal seasonal mean departure of AIR. In Table 2 the seasonal mean values of the PC's are a proxy for residence time. For the $\overline{PC's}$, positive (negative) departures indicate that the preferred location for convection is over (south of) the Indian subcontinent (Fig. 8). From Table 2 we see that in both 1987 and 1988 $\overline{PC-1}$ is negative, thus the 30-60 day mode could not have been responsible for the changes in the wind and rainfall over India. The same is the case for $\overline{PC-2}$ and $\overline{PC-4}$, the latter of which is incorrectly phased to give the proper interannual signal over India. Only $\overline{PC-3}$ has the correct phasing to give the below-normal (above-normal) rainfall over India in 1987 (1988). Goswami et al. (1998) then state "For the rest of the ten-year period, the relationship (between residence time and AIR) is not very strong." Their relationship is weak because, as demonstrated above, only 1 of the first 4 modes is systematically perturbed by AIR. PC's 1, 2 and 4 vary randomly with respect to AIR (Fig. 11) and since these modes were

included in their estimated residence time, the relation to AIR is necessarily weak. The preponderance of evidence presented in Sections 4a-b indicates that it is the variations of EOF-3/PC-3 that consistently exert the most systematic control over the subseasonal and interannual variations of 850hPa circulation and rainfall over India during most years. Further details regarding the interactions of the various modes, and their influence on seasonal mean rainfall will be presented in Section 5.

If a link between the variations of the PC's and the boundary forcing were established, then there would be the prospect for seasonal predictability in a probabilistic sense. With the implementation of the Tropical Ocean Global Atmosphere Tropical Atmosphere Ocean (TOGA TAO) array our ability to forecast ENSO has improved (McPhaden 1999). Hence, it is prudent to investigate if ENSO influences the dominant modes of ASM variability. Figure 12 shows the standardized PDF's for all years, and for El Niño and La Niña years when the standardized NINO3 anomalies exceed the +/-0.5 standard deviation thresholds (Fig. 2a). PC-2 is systematically perturbed under the influence of the ENSO boundary forcing. During El Niño years, the mean of PC-2 is biased towards negative loadings, corresponding to anticyclonic circulation and drier conditions in the vicinity of northern India, the Bay of Bengal, and southeast of China (Fig. 6b). Conversely, these regions are pre-disposed towards cyclonic conditions and are wetter during La Niña years. Significance testing indicates that the mean of the La Niña PDF is greater than the mean of the El Niño PDF at better than the 2.5% significance level. Thus, for EOF-2/PC-2 there is the potential for predictability in a probabilistic sense if a priori information regarding the future state of ENSO is available. The result that ENSO perturbs EOF-2/PC-2, while AIR is systematically controlled by EOF-3/PC-3 is consistent with the lack of a unique relationship between NINO3 SST and AIR (Figs. 2a-b), their correlation being -0.46.

It is interesting that only one of the modes that contributes to the northward propagation of the TCZ is affected by the ENSO boundary forcing. This does not preclude the possibility of northward propagation. In fact the summer of 1987 was characterized by strong northward propagations along the monsoon trough (Annamalai et al. 1999). As seen in Table 2, the seasonal mean of PC-2 is biased negative, the seasonal mean being -7.11. This is consistent with the probabilistic influence of the boundary forcing based on the PDF's for El Niño versus La Niña years (Fig. 12b). However, as discussed above, the other dominant modes analyzed do not exhibit systematic perturbations related to ENSO boundary forcing. Of course it is the interactions of the different modes of variability that is important in determining the overall performance of the ASM. A random bias to one of the other chaotic subsea-
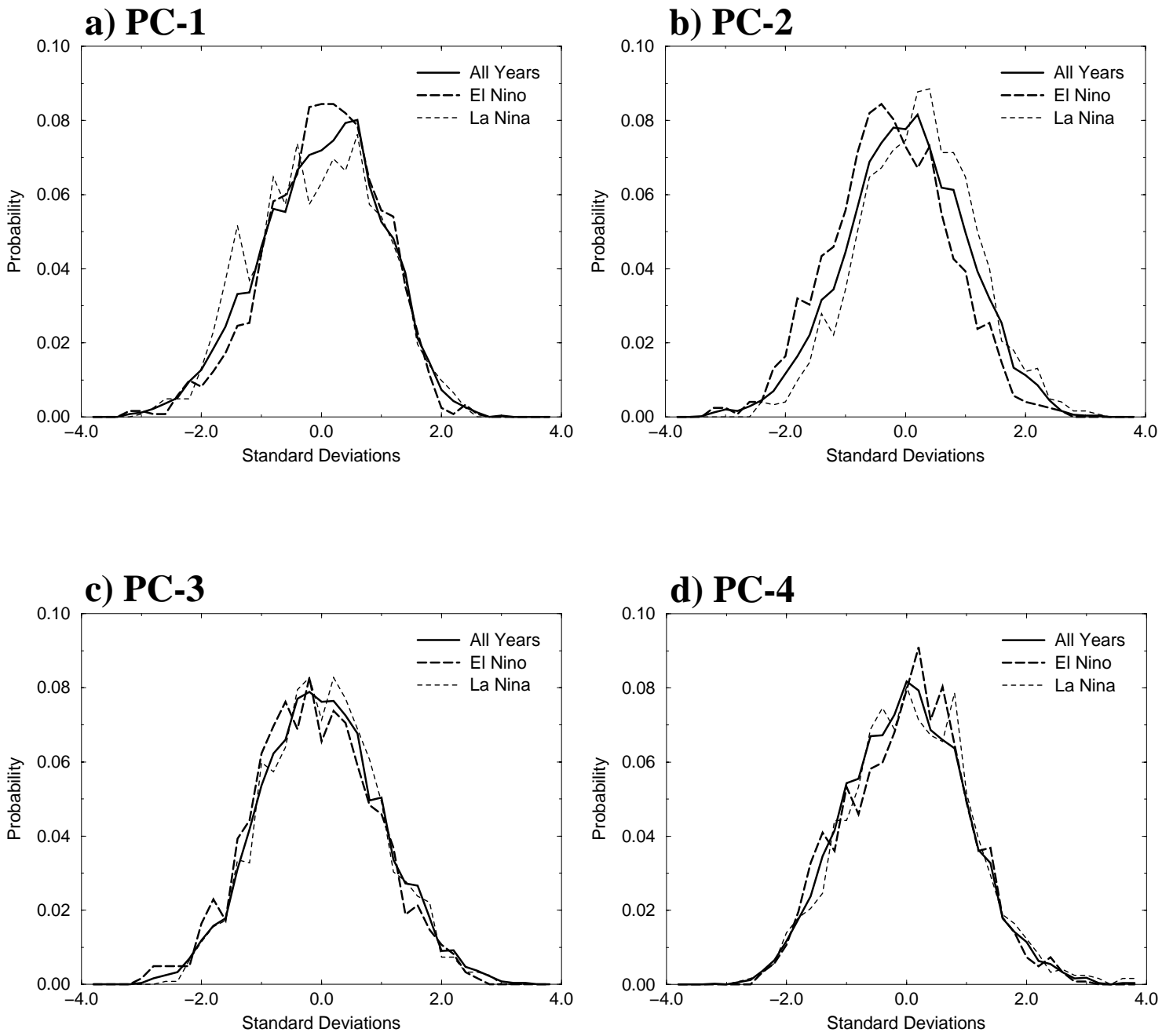
Figure 12: As Fig. 11 but for stratification based upon the NINO3 SST index given in Fig. 2a.

sonal modes during a given ENSO event might either exacerbate or counteract the systematic perturbation of EOF-2. 1987 is an excellent example of constructive interference of the dominant modes. As expected PC-3 is also biased towards negative values (Table 2), consistent with the afore-mentioned AIR PDF partitioning (Fig. 11c). However, PC-1 is also strongly negative (Table 2). The result of our partitioning by the boundary forcing in Fig. 12a indicated that this mode was unaffected by NINO3 SST. Rather EOF-1/PC-1 is chaotic with respect to the ENSO boundary forcing. Thus, by chance occurrence this mode was biased negatively during this year, and given its relationship to rainfall (Figs. 8a and 9a) a negative bias is consistent with below normal AIR (and below normal rainfall across the continental ASM region). This suggests that the expected below normal AIR associated with EOF-3/ PC-3, and the boundary forcing influence of EOF-2/PC-2 has been exacerbated through the chance occurrence that EOF-1/PC-1 was also biased negatively during this year, thus resulting in one of the most intense weak AIR years on record. This underscores the probabilistic nature of these relationships, and emphasizes the role that internal dynamics plays in determining the behaviour of the monsoon system (Goswami 1994). This, coupled with the small percentage variance explained by EOF-2 is indicative of the complexity of the monsoon system, and the difficulty that arises in its seasonal prediction.

In Fig. 5 we noted an interdecadal signal in the land-sea temperature contrast. As seen in Fig. 13c, PC-3 is systematically perturbed towards negative values during years of weaker land-sea temperature contrast (positive values of SST/tg in Fig. 5b), whereas it is perturbed towards positive values during years of stronger land-sea temperature contrast (negative values of PC-1 in Fig 5b). These changes in the means of the PDF's are significant at the 5% level (single-sided t-test). Thus, during the early portion of the record when the land-sea temperature contrast was enhanced and the DMI was stronger (Fig. 2c), the PDF of PC-3 is biased towards positive values (Fig. 13c), consistent with enhanced rainfall in the vicinity of India. Conversely, during the latter portion of the record when the land-sea temperature contrast is weaker and the DMI is weaker, the PDF of PC-3 is biased towards negative values consistent with below normal rainfall in the vicinity of India. The changes in the PDF's of PC-1 and PC-4 (Figs. 13a and 13d) are consistent with the stronger (weaker) DMI being associated with stronger (weaker) land-sea temperature contrast, although the differences in the means are not statistically significant, even for a one-tailed t-test at the 5% significance level. The perturbation to PC-3
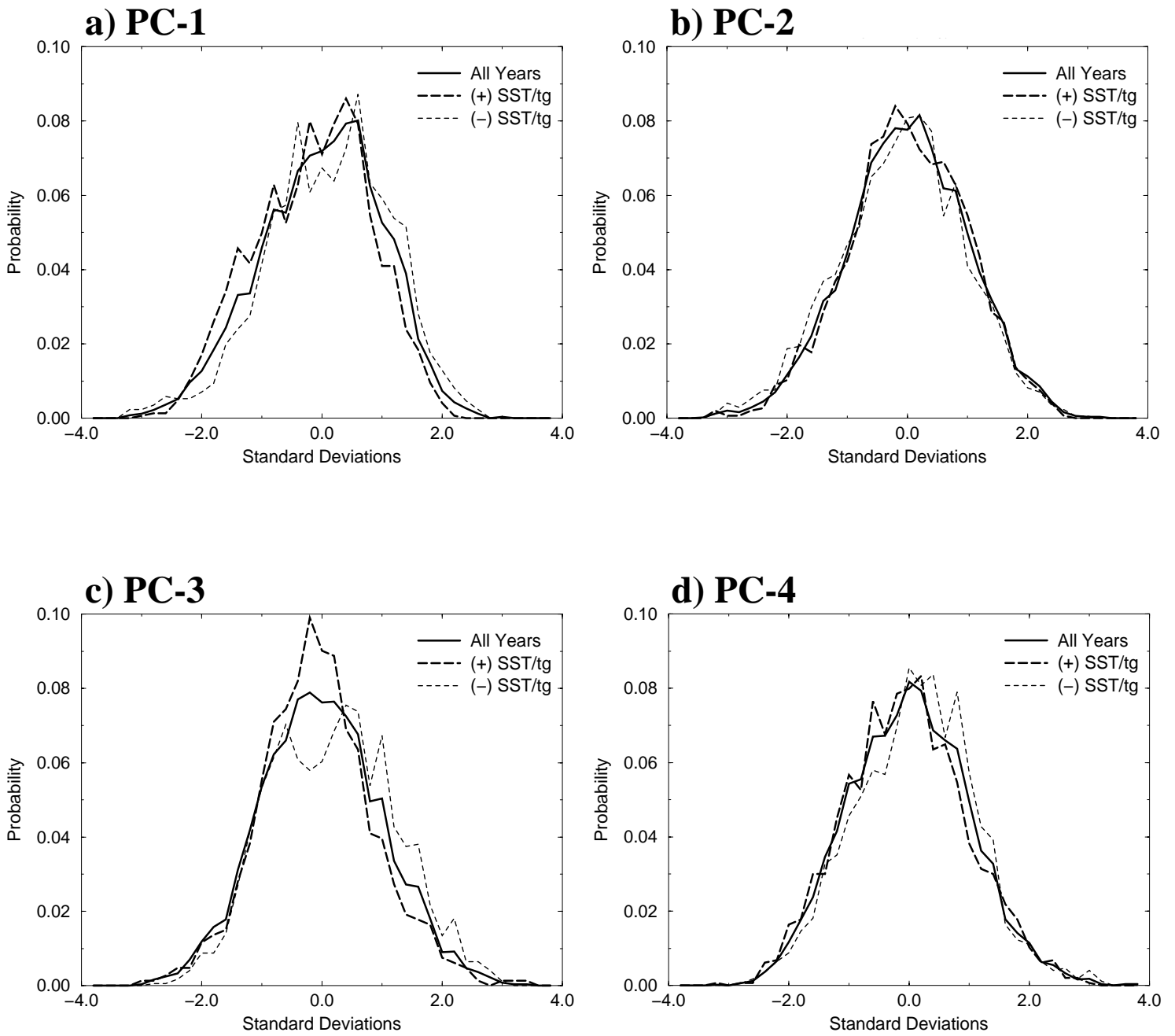
Figure 13: As Fig. 11 but for stratification based upon PC-1 of the observed SST and NCEP/NCAR surface temperature over land for Asian summer monsoon region given in Fig. 5b.

indicates that the Indian Ocean SST plays an important role for interdecadal variations of the ASM.

With respect to the DMI (Fig. 2c), the means of the PDF's 1-3 (Fig. 14a-c) are biased towards positive (negative) loadings for years of enhanced (weakened) vertical windshear. However, the differences in means are not significant at the 2.5%, or the 5% level for a one-sided t-test. Even so, the biases to these PDF's are consistent with that expected due to the interdecadal variability of the DMI.

The results presented indicate that the summer monsoon is not dominated by a single mode of variability. Moreover, the partitioning of the PDF's of the PC's indicate that only a subset of the modes are systematically perturbed, and in the case of ENSO forcing only PC-2 is influenced. These two factors conspire to complicate the prospect for dynamical seasonal predictability of the ASM.

Importantly, this observationally based study clearly indicates that the PDF's are generally Gaussian in shape, and that the perturbations are realized as changes in the means of the distributions. However, results from simple models indicated that systematic changes in the shape of the PDF of the subseasonal mode were manifested as bimodality (Palmer 1994, Webster et al. 1998). This indicates that these models are failing to capture processes and interactions that are important for ASM variability. If it is also the case that NWP/general circulation models have similar shortcomings, then improvements of model formulation will increase the prospect for seasonal forecasting.

c) The Role of the Basic State

While the power spectra of the modes presented in Fig. 6 are dominated by subseasonal timescales (Fig. 7), the variations are nevertheless superimposed upon interannual/decadal variations associated with the slowly varying boundary conditions due to a changing basic state, since the data employed have not been filtered (other than to remove the climatological daily values). A question of interest is: Are the basic spatial and temporal characteristics of the modes presented in Fig. 6 fundamentally affected by variations of timescales longer than one season? To investigate this question we have recalculated EOF's for the same data used in Fig. 6, but prior to the analysis we have highpass filtered the data with a 90-point Lanczos filter that has half-power at 100 days. Thus, we retain all variations that are statistically significant at the 5% level relative to a rednoise background (Fig. 7).

The resulting EOF patterns using the filtered data are given in Fig. 15. Relative to the unfiltered data in Fig. 6, EOF-1 and EOF-4 are modified little, and the correla-
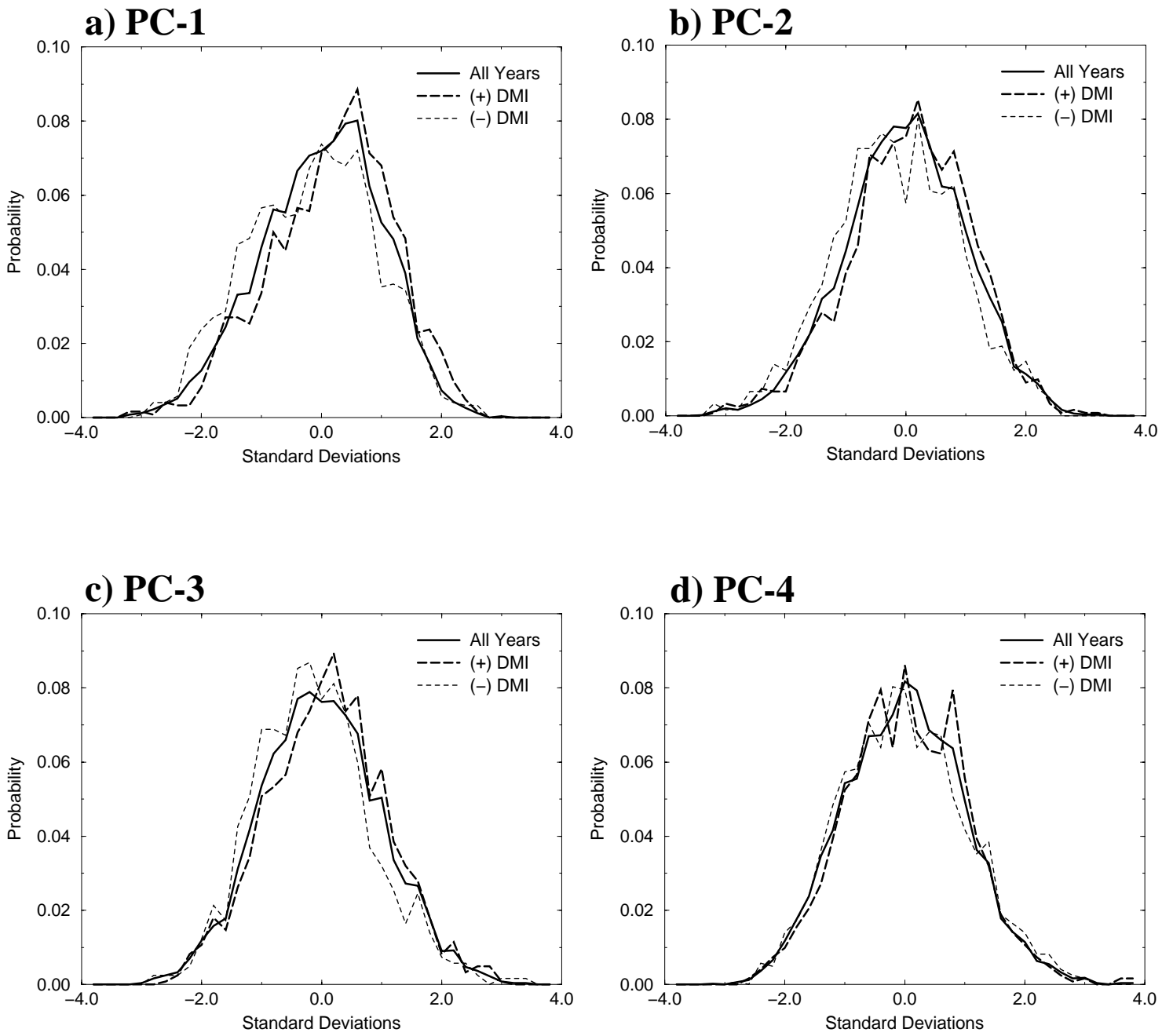
Figure 14: As Fig. 11 but for stratification based upon the dynamical monsoon index given in Fig. 2c.

tions of the unfiltered and the filtered PC time series are 0.93 and 0.94 respectively for the 40 summers of daily data. This indicates that for the unfiltered and filtered data the spatial/temporal characteristics of these modes are in large part nearly identical, indicating these to be normal modes of the summer monsoon system. Substantial modifications occur to EOF-2, the mode that showed a statistically significant link to the phase of ENSO. For the filtered version of EOF-2, absent are the "closed" cyclonic flows over the Bay of Bengal, and over China and the South China Sea. The primary change to EOF-3 is a shift of the anticyclonic anomalies towards the southern Bay of Bengal. For PC-2 and PC-3 the correlations of unfiltered and filtered time series are somewhat lower relative to the modes that were unchanged, being 0.75 and 0.73 respectively, indicating that the basic state is modifying the spatio-temporal variability of these modes.

The influence of the basic state on the PC's is clearly demonstrated in Fig. 16. Here we show the PC's of the filtered and unfiltered data for June-September 1987, an El Niño year with weak AIR and weak DMI (Fig. 2). During this year the high-frequency temporal variations of the filtered and unfiltered data are nearly identical, especially for PC-1 and PC-4. However, as discussed in Section 4b, PC's 1-3 from the unfiltered data are negatively biased as seen in Table 2. Filtering the data has resulted in removal of the low-frequency basic state variations that give rise to the substantial offsets of the unfiltered data (Table 2). Alternatively, the filtered data have much smaller offsets, as seen in Table 3.

The changes to the temporal variations of the filtered data are evident in their PDF's. The most important change that occurs with the use of filtered data is the absence of statistically significant changes to the PDF's with respect to ENSO, ASM SST and ground temperature, and AIR. For example, the PDF's of the filtered data partitioned according to ENSO are given in Fig. 17. The PDF's are still approximately Gaussian, but no evidence of a systematic perturbation by the boundary forcing is evident because the bias due to the low-frequency basic state has been removed. This bias is responsible for the perturbations of the PDF's seen in Figs. 11-14. This indicates that the slowly varying component of the climate system is responsible for the perturbations in the means of the PDF's described in Section 4c. Thus, an accurate forecast of the basic state is a prerequisite for probabilistic forecasts of the subseasonal modes. The importance of the basic state is investigated further in the next section, in which we evaluate the projection of the subseasonal modes on to the interannual variations of the low-level flow and rainfall.
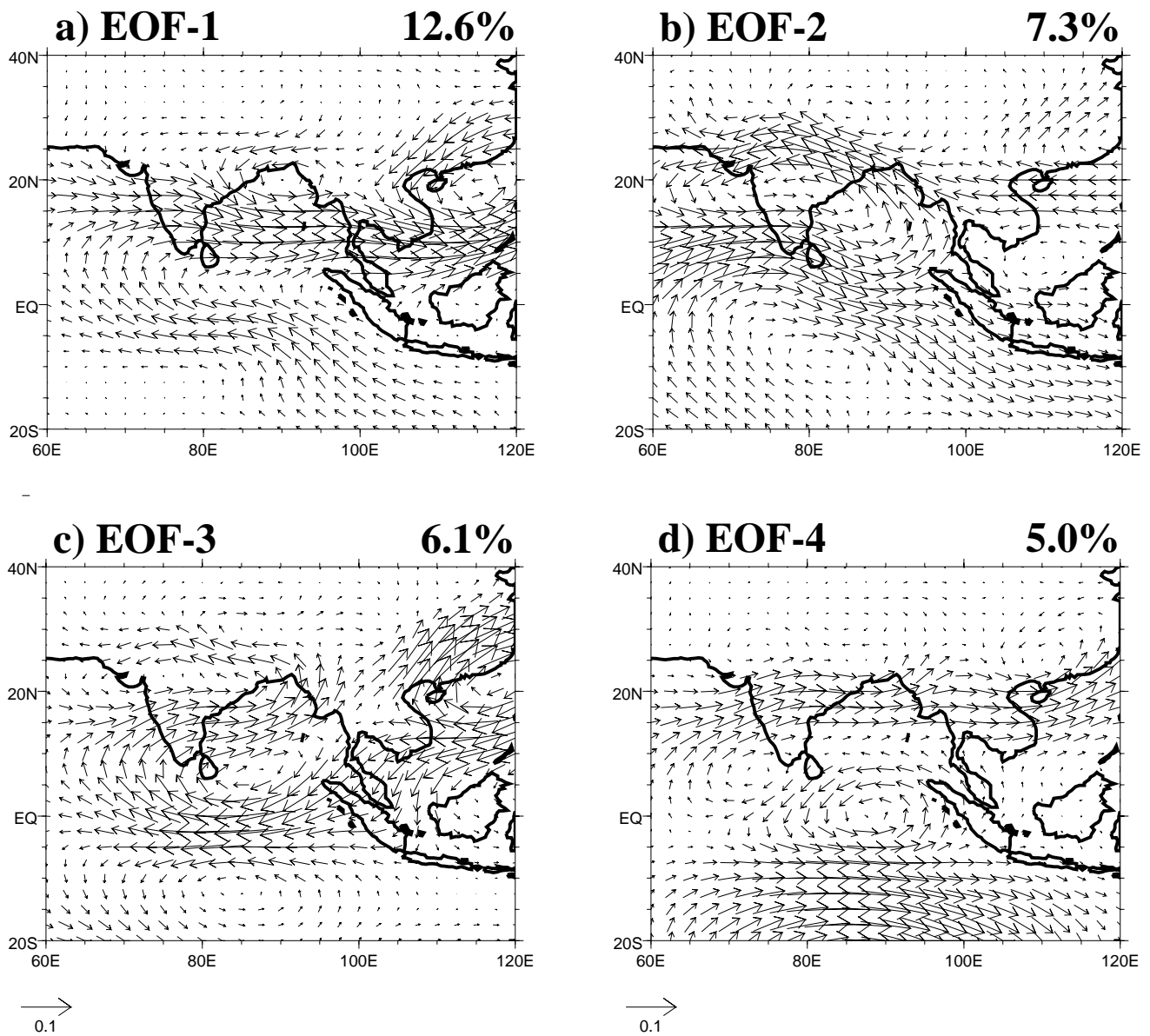
Figure 15: Results of an EOF analysis of NCEP/NCAR daily 850hPa wind anomalies for June-September 1958-97. Prior to the analysis the climatological daily means have been removed and the data were subjected to a 90-point Lanczos highpass filter to isolate time-scales less than 100 days. (a) EOF-1, (b) EOF-2, (c) EOF-3, (d) EOF-4. The percent variance explained by each mode is also given.
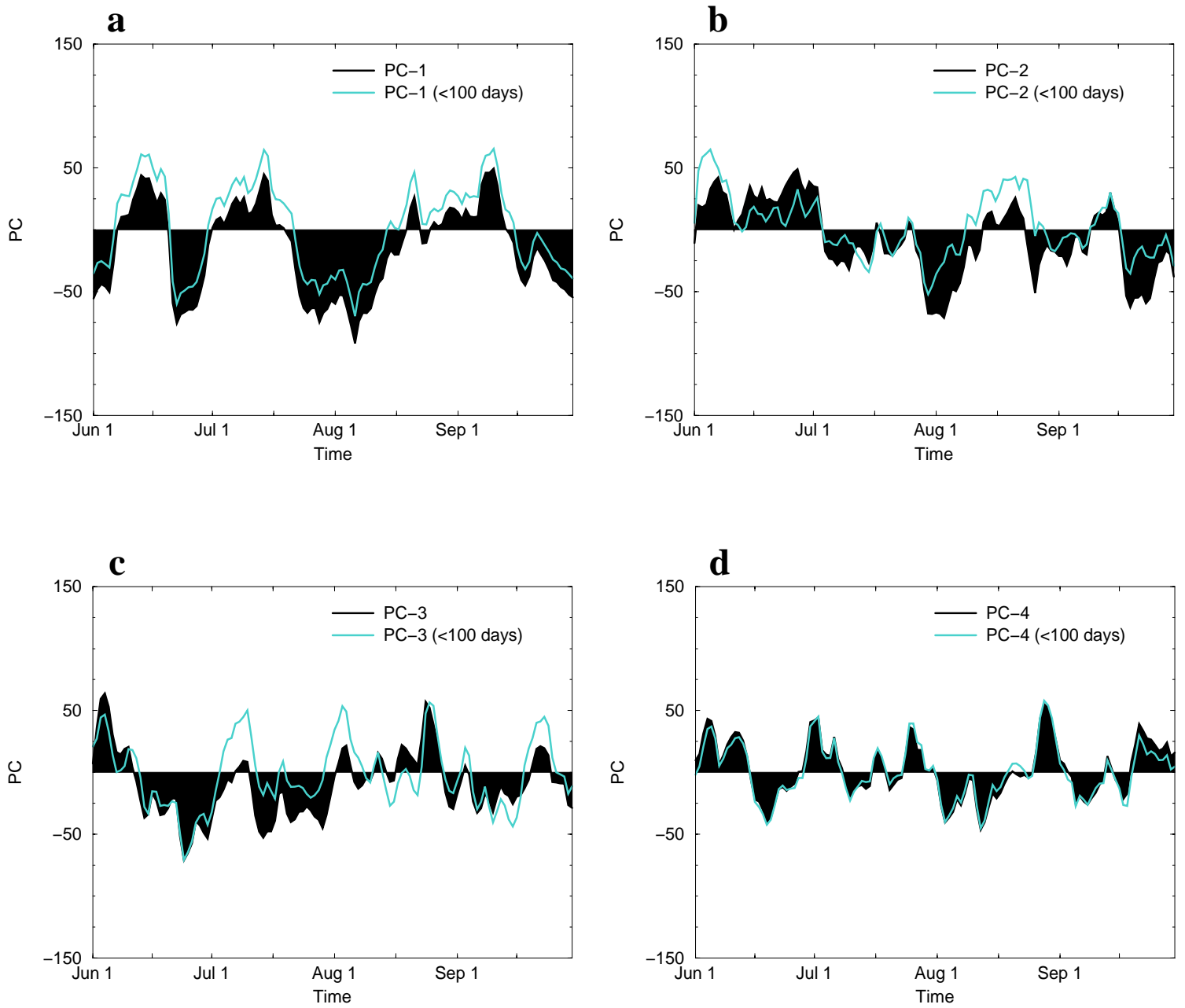
Figure 16: For 1987 the principal components for the unfiltered EOF's in Fig. 6 are given as the filled black curves, while the principal components of the filtered EOF's in Fig. 15 are given as the light-shaded lines.

-34-

Table 3: Seasonal means (June-September) of the principal components of the highpass filtered daily 850hPa wind for 1958-97. The associated EOF patterns are presented in Fig. 15.

| Year	$\overline{PC\text{-}1}$	$\overline{PC\text{-}2}$	$\overline{PC\text{-}3}$	$\overline{PC\text{-}4}$	Year	$\overline{PC\text{-}1}$	$\overline{PC\text{-}2}$	$\overline{PC\text{-}3}$	$\overline{PC\text{-}4}$
1958	2.9	-2.6	0.5	-0.4	**1978**	-1.7	1.2	1.1	-0.7
1959	0.2	-1.0	1.1	-2.4	**1979**	-3.4	1.8	0.9	-1.4
1960	-0.9	-0.8	-1.3	-1.2	**1980**	0.0	1.3	0.8	-0.4
1961	-1.1	-2.0	2.1	2.7	**1981**	3.1	2.1	-0.3	-1.8
1962	3.4	-3.1	2.5	0.1	**1982**	1.4	3.0	-2.3	1.3
1963	4.1	-2.3	-0.2	-0.4	**1983**	0.1	-0.6	1.3	-1.3
1964	-0.2	-0.4	1.2	0.6	**1984**	-1.1	0.3	1.1	-0.8
1965	1.9	-0.9	-0.6	1.5	**1985**	1.5	-2.9	-1.5	1.5
1966	-2.1	-0.5	0.0	0.8	**1986**	-1.9	0.2	0.7	-0.8
1967	-1.1	-0.5	-0.5	0.0	**1987**	2.5	3.2	-1.1	1.1
1968	0.8	0.8	-0.6	-1.4	**1988**	0.1	0.1	3.4	-1.6
1969	1.8	0.6	-0.9	0.6	**1989**	-2.5	-2.2	3.1	1.9
1970	0.9	0.5	-0.5	0.3	**1990**	-1.0	-0.6	-1.7	-1.0
1971	1.1	-1.1	1.1	0.3	**1991**	0.7	2.0	-3.4	0.7
1972	-1.9	1.1	-2.3	-0.8	**1992**	-3.0	0.3	-1.6	0.1
1973	-1.4	0.9	-0.4	1.9	**1993**	-1.2	0.9	-0.7	1.7
1974	-1.8	-2.5	0.4	-0.3	**1994**	0.4	2.1	-2.4	0.8
1975	0.1	-0.4	0.8	-1.7	**1995**	-0.3	0.4	-0.9	0.6
1976	0.4	0.0	0.2	-0.3	**1996**	-0.8	0.9	0.4	0.1
1977	0.8	1.6	-1.0	0.1	**1997**	-1.1	-0.7	1.1	-0.6
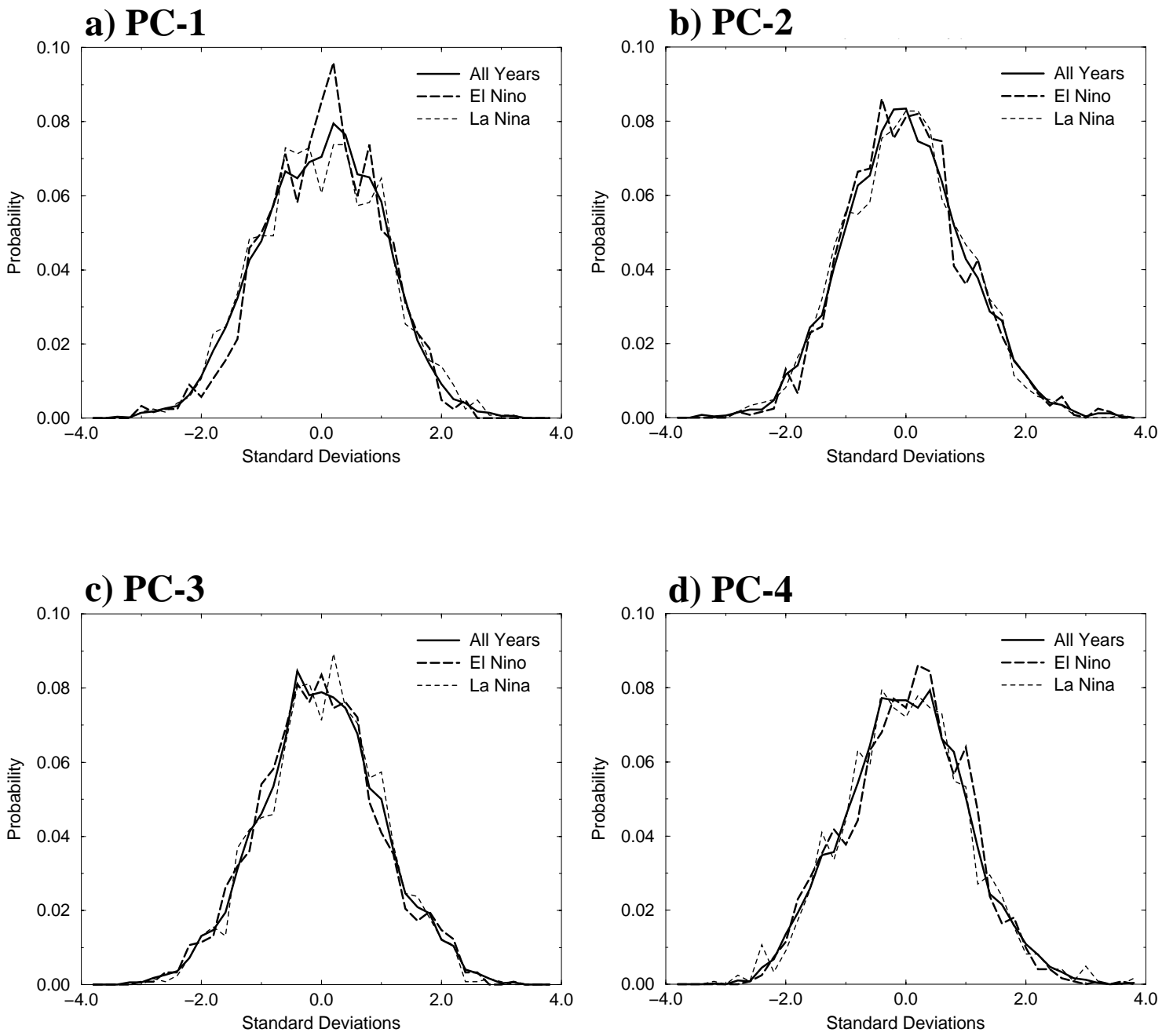
Figure 17: As Fig. 11 but for stratification of the principal components of the highpass filtered data based upon the NINO3 SST index given in Fig. 2a.

5. Reconstruction of the Interannual Variability from the Subseasonal modes

Figures 11-14 indicate that a very limited number of modes are perturbed systematically on timescales where demonstrated forecast prospects exist (i.e., ENSO). As discussed in the section 4b, the seasonal means of the principal components give the contribution of that mode to the total seasonal anomaly. These seasonal mean PC values, multiplied by their respective EOF patterns, and then summed over n patterns yield a reconstructed seasonal anomaly, which can be compared to the total seasonal anomaly (calculated using monthly data relative to the 40-year climatology). In this manner we can investigate how well the dominant modes of subseasonal variability relate to the interannual variability. Importantly, we can also examine the role of the basic state by comparing the reconstructions of the unfiltered and filtered data.

To reconstruct the precipitation anomalies, the daily PC's have been linearly regressed against daily anomalies of reanalysis precipitation. The regressed fields multiplied by the seasonal mean PC values are summed to yield a reconstructed seasonal anomaly. The reconstructions are validated against the total seasonal anomaly (calculated using monthly data relative to the 40-year climatology), and when possible also against the observationally based rainfall estimates of Xie and Arkin (1996).

During 1987, a weaker than normal Somali jet persisted throughout much of summer (Krishnamurti et al. (1989). This is confirmed in Fig. 18 which shows the total and reconstructed 850hPa anomalies for 1987. The basic structure of the total anomalies (Fig. 18a) is captured in the reconstruction using EOF's 1-4 (Fig. 18b). The easterly anomalies from 5⁰N-15⁰N, the cyclonic anomalies south of the Indian subcontinent, and the anticyclonic circulation over northern India and over the South China Sea are captured reasonably well. However, the reconstruction fails to reproduce many of the details of the total anomaly, particularly north of 30⁰N and south of the equator where the magnitudes of the wind vectors are greatly underestimated. This indicates that in order to capture the details of the flow a larger number of EOF's would be required in the reconstruction. The reconstruction using EOF's 1-4 of the filtered data is presented in Fig. 18c. Consistent with the small seasonal mean values of the filtered PC's (Table 3), a factor of 10 difference in the length of a unit vector is required to show the reconstructed anomalies. Moreover, the reconstruction using the filtered data does not even qualitatively agree with the total anomaly field. This indicates the dominant role that the low-frequency basic state plays in setting up the large-scale and regional-scale circulations.
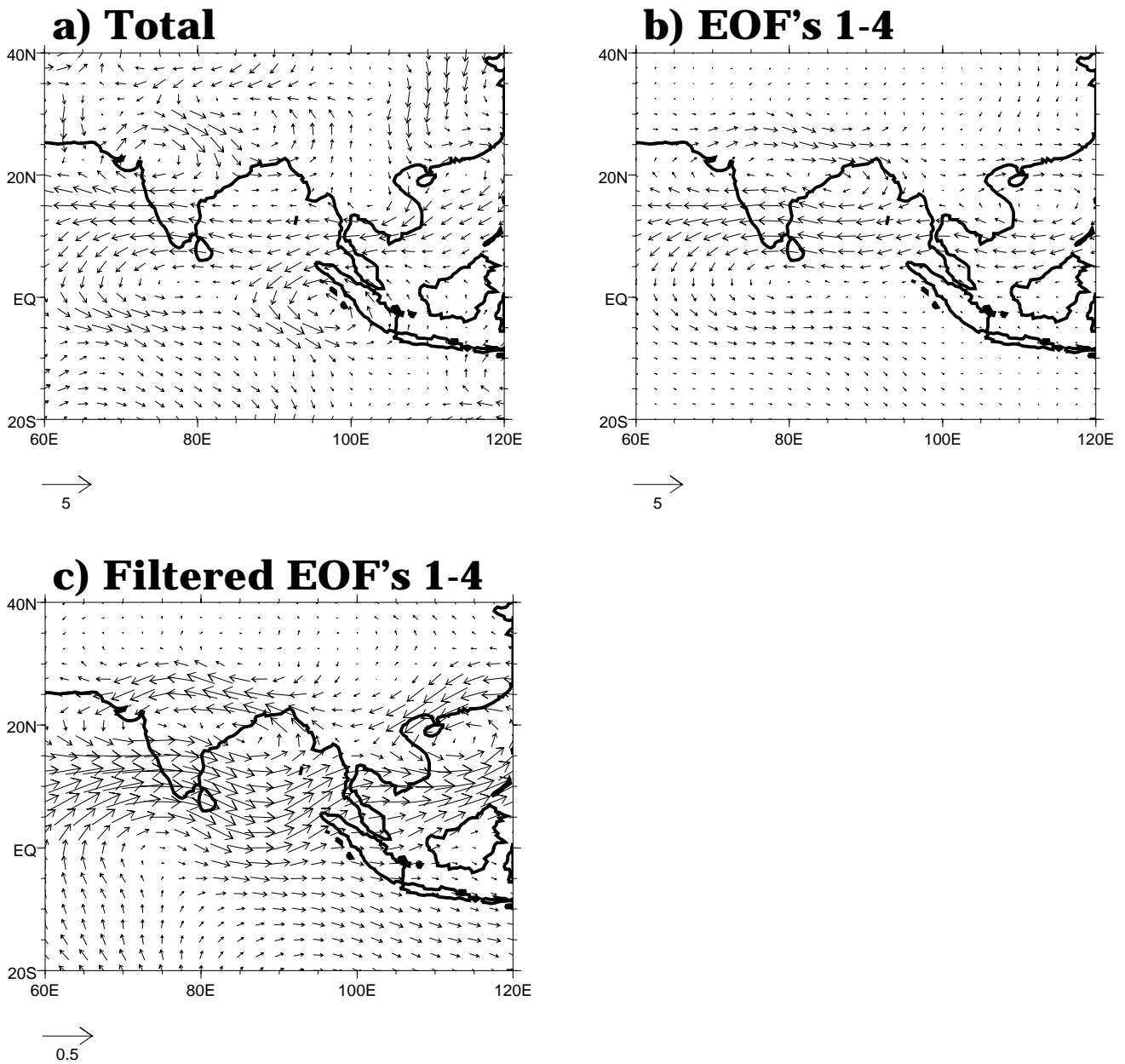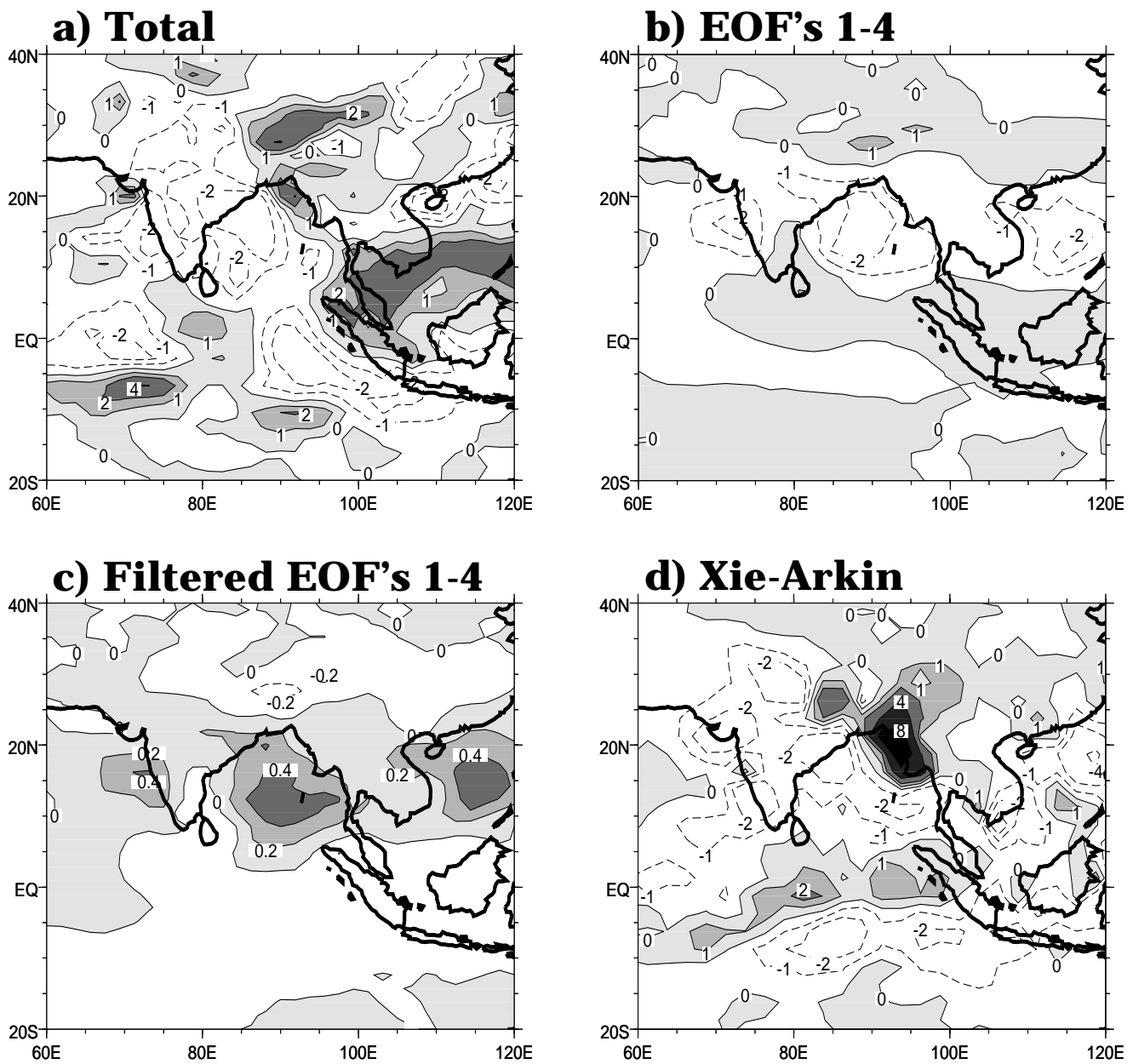
a) Total

b) EOF's 1-4

c) Filtered EOF's 1-4

Figure 18: The seasonal mean (June-September) 850hPa wind anomaly (ms^{-1}) for 1987 with respect to the base period 1958-97 (a) the total, (b) reconstructed based on the product of the unfiltered EOF's in Fig. 6 and the seasonal mean PC values in Table 2, (c) reconstructed based on the product of the filtered EOF's in Fig. 15 and the seasonal mean PC values in Table 3. Note: the small magnitude of the reconstructed anomalies from the filtered data in (c) requires a unit vector of 0.5ms^{-1}, whereas the total and unfiltered reconstructions in (a) and (b) have unit vectors of 5ms^{-1}.

a) Total
b) EOF's 1-4
c) Filtered EOF's 1-4
d) Xie-Arkin

Figure 19: The seasonal mean (June-September) precipitation anomaly (mm day^{-1}) for 1987 with respect to the base period 1958-97 (a) the total from NCEP/NCAR reanalysis, (b) reconstructed based on linear regressions of the daily unfiltered PC's of the EOF's in Fig. 6 and daily precipitation anomalies. The reconstruction presented is the product of the linear regressions and the seasonal mean PC values in Table 2, (c) reconstruction based on linear regressions of the daily filtered PC's of the EOF's in Fig. 15 and daily precipitation anomalies. The reconstruction presented is the product of the linear regressions and the seasonal mean PC values in Table 3, (d) the total from the observed dataset of Xie and Arkin (1996). Note: the observed anomalies are calculated with respect to the base period 1979-95. For (a), (b) and (d) contours are plotted at 0, +/- 1, 2, 4, 8,... mm day^{-1}. For (c) contours are plotted at 0, +/- 0.2, 0.4, 0.8, 1.6,... mm day^{-1}. In all cases shading is used to indicate positive anomalies.

The total and observed rainfall anomalies for 1987, shown in Figs. 19a and 19d, are in good agreement, with below normal rainfall over India and most of the Bay of Bengal. Enhanced rainfall is strongest over the northeastern Bay of Bengal and Burma and in a narrow band in the equatorial Indian Ocean. The reconstructed rainfall anomalies in Fig. 19b are qualitatively consistent with the observations and the total forecast field in representing the deficit rainfall, but it fails to produce the enhanced rainfall near Burma. This inconsistency is not surprising since the reconstructed flow fails to capture the onshore westerly flow in this region (Fig. 18b). This is further evidence that the interannual variability of the ASM is not dominated by a few modes of variability, and that higher order modes are necessary to capture regional-scale features. Concomitant with the incorrect reconstruction of the filtered winds (Fig. 18c) the rainfall reconstruction based on the filtered anomalies is incorrectly simulated (Fig. 19c), including magnitudes that are about a factor of five smaller than the unfiltered reconstruction. As seen in Fig. 16, the filtered and unfiltered principal components have nearly identical amplitudes, and their regressions against the rainfall yield similar linear fits (not shown). However, from comparing Tables 3 and 2, the seasonal means of the filtered principal components are much smaller than those from the unfiltered data because the low-frequency component has been removed. With the smaller seasonal mean values, the filtered data do not project as strongly on to the interannual variability, thus the reduced magnitude of the filtered reconstructions relative to the unfiltered reconstructions. Additionally, the relative loadings of the filtered PC's (Table 3) are not consistent with the unfiltered PC's (Table 2) thus resulting in the incorrect representation of the wind and rainfall anomalies in the filtered reconstructions. The basic state is so important that its' removal precludes even a qualitative representation of the total anomalies.

MONEG spent much time evaluating the 1988 ASM, which occurred during strong La Niña conditions. In particular, the monsoon over India was modulated primarily through perturbations along the monsoon trough (Fig. 20a). This proves to be a curious year since even though this was the strongest La Niña in the 40-year record (Fig. 2a), the seasonal mean of PC-2 is negative, contrary to the systematic perturbation of its PDF in Fig. 12b, which indicates PC-2 to be biased towards positive values under La Niña conditions. This exemplifies the nature of probabilistic relationships, which sometimes do not manifest as expected. The reconstruction using EOF's 1-4 (Fig. 20b) gives rise to the basic easterly anomalies seen in the total (Fig. 20a), but it fails dramatically over China. Inclusion of higher order subseasonal modes that are associated with variations of the Mei-Yu front lead to an improved
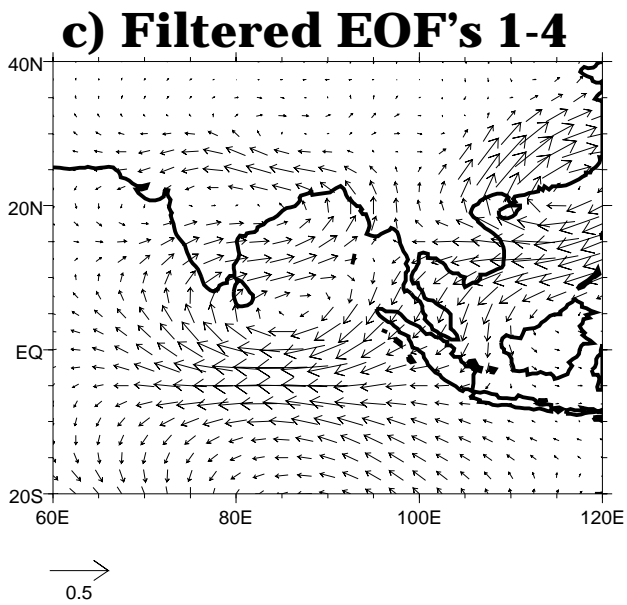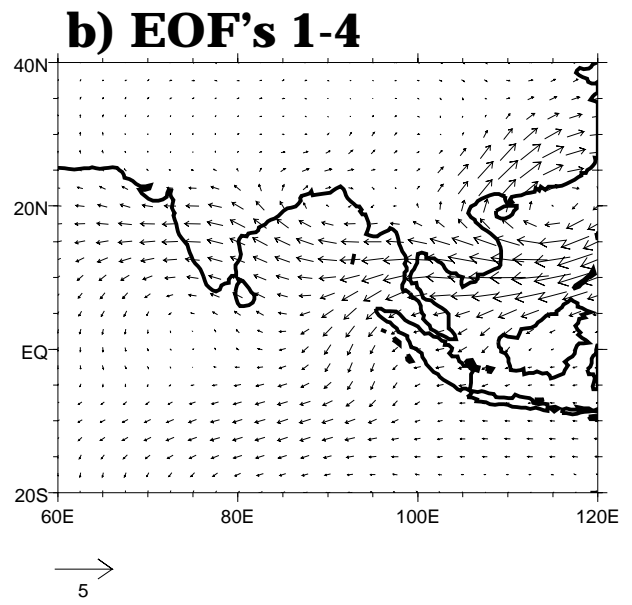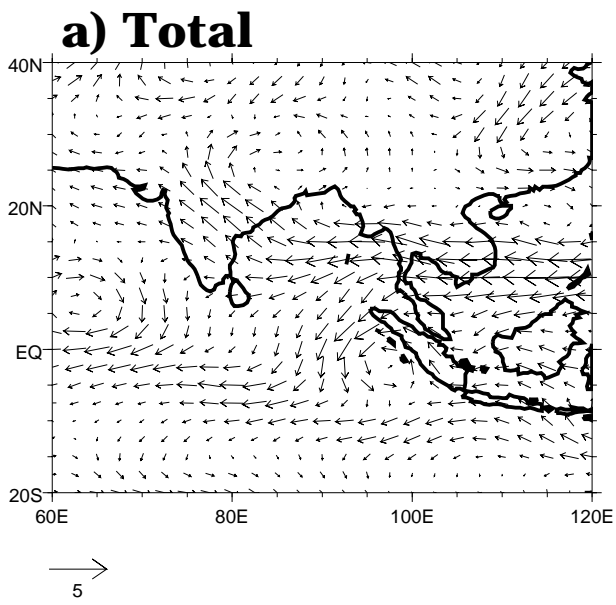
a) Total

b) EOF's 1-4

c) Filtered EOF's 1-4
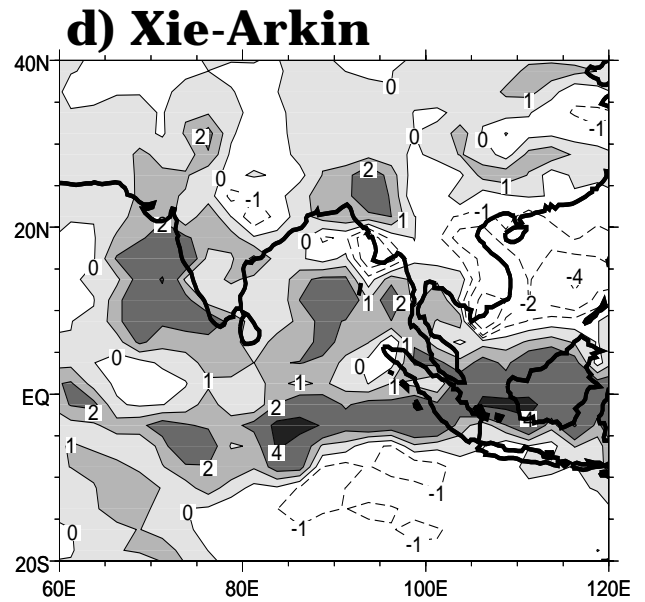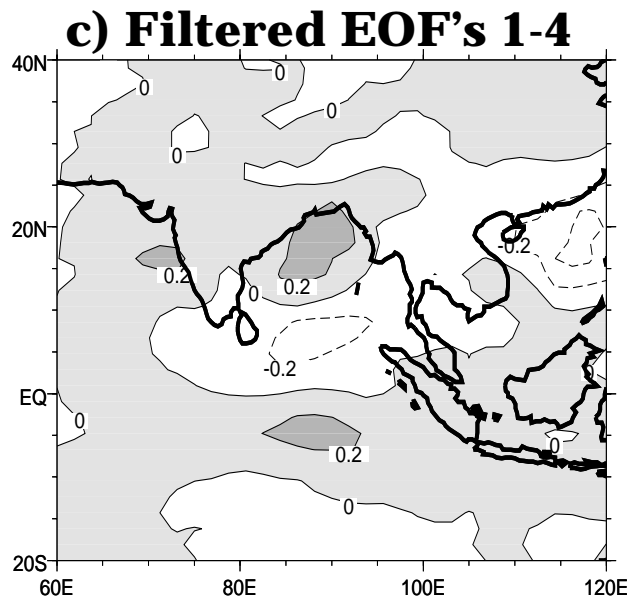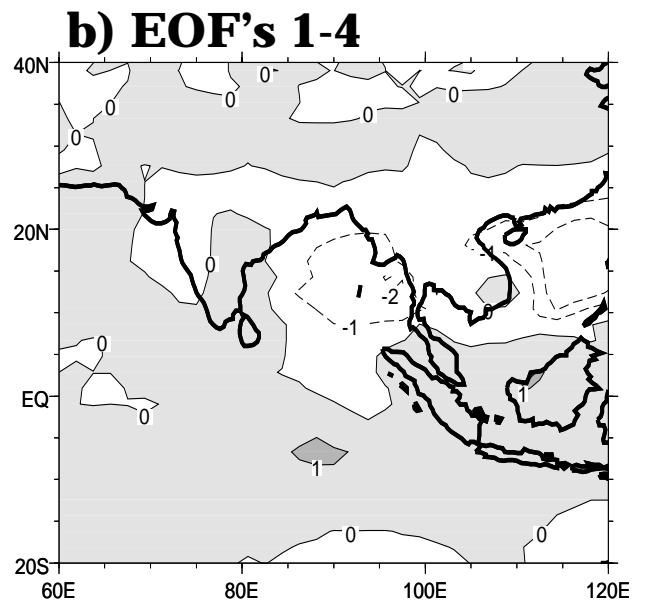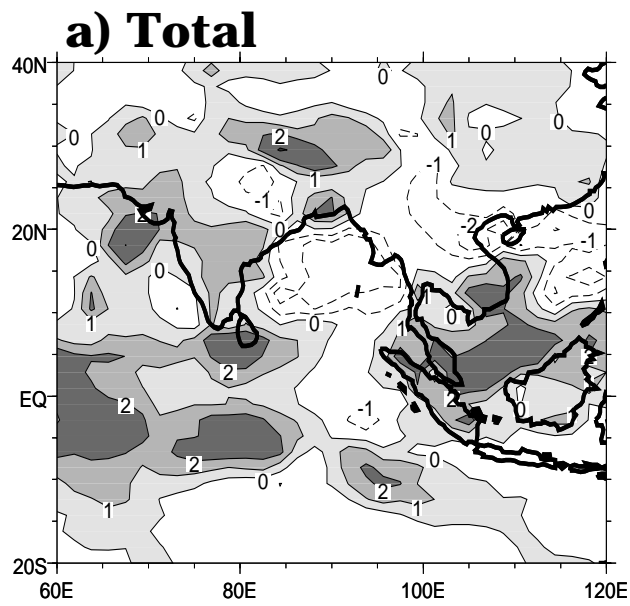

Figure 20: As Fig. 18 for 1988.

Figure 21: As Fig. 19 for 1988.

reconstruction of the wind anomalies over China (not shown). The precipitation composites of these higher order modes are similar to the modes of high cloud discussed in Kang et al. (1999). As for 1987, the magnitudes of the wind vectors are too weak outside of the core region of the ASM, and the reconstruction using the filtered data (Fig. 20c) is inconsistent with respect to the total anomaly.

The total forecast and observed rainfall anomalies for 1988, shown in Figs. 21a and 21d, are in qualitative agreement. The reanalysis fails to capture the positive anomalies off the west coast of India, and the anomalies over much of the Bay of Bengal and the eastern equatorial Indian Ocean are underestimated. This reduces the prospect for reconstruction, and indeed as seen in Fig. 21b these inconsistencies are manifest in the unfiltered reconstruction. Additionally, shortcomings in the reconstructed wind (Fig. 20b), such as the poor penetration of the monsoon trough into northwestern India, contribute to the poor representation of the reconstructed rainfall over the Indian subcontinent. While the rainfall reconstruction using the filtered data (Fig. 21c) appears more favorable, albeit with unduly small rainfall rates, inspection of Fig. 20c indicates that the qualitatively correct rainfall representation is obtained for the wrong reason since the reconstructed wind using the filtered data is incorrect.

1994 is an interesting year since it has a strong AIR signal, but the ENSO boundary forcing and DMI were very weak (Fig. 2). Compared with 1988 (Fig. 20), another year of enhanced AIR, the anomalous flow is radically different (Fig. 22), underscoring the wide variety of flow regimes under which regional rainfall can be significantly affected. EOF's 1-4 capture the large-scale features of the total anomalies (Fig. 21b), but again the absence of higher order modes precludes the representation of regional-scale features. The filtered reconstruction is incorrect (Fig. 22c).

In 1994 the reanalysis gives a very good representation of the observed rainfall anomalies, as seen in Figs. 23a and 23d respectively. The problematic regions include the eastern equatorial Indian ocean, the southern South China Sea and east of southern India where the reanalysis generates positive rainfall anomalies. Qualitatively, the reconstructed rainfall in Fig. 23b is in good agreement with the total anomalies. However, the reconstructed rainfall anomalies are underestimated over Burma, Thailand and Laos where the reconstructed winds poorly represent the convergence of the northeasterlies and westerlies near 20°N. Additionally, relative to the total anomalies, the reconstructed rainfall is overestimated along the west coast of India near 15°N (though not with respect to the observed anomalies), as the total low-level flow is more divergent relative to the reconstructed flow. What agreement

a) Total

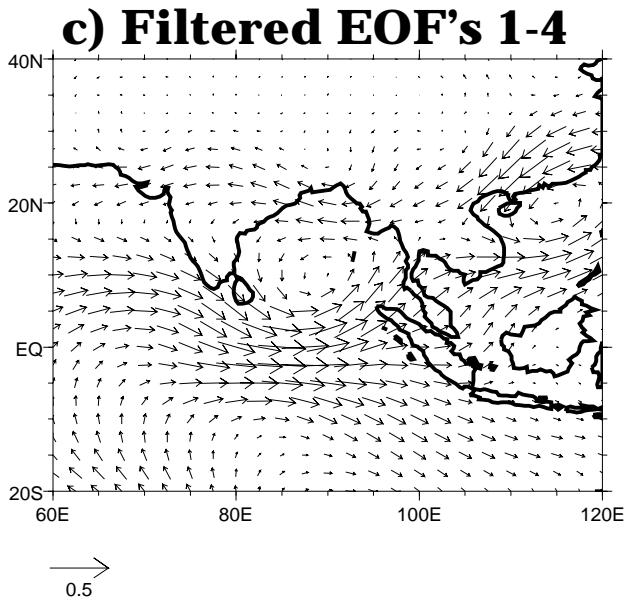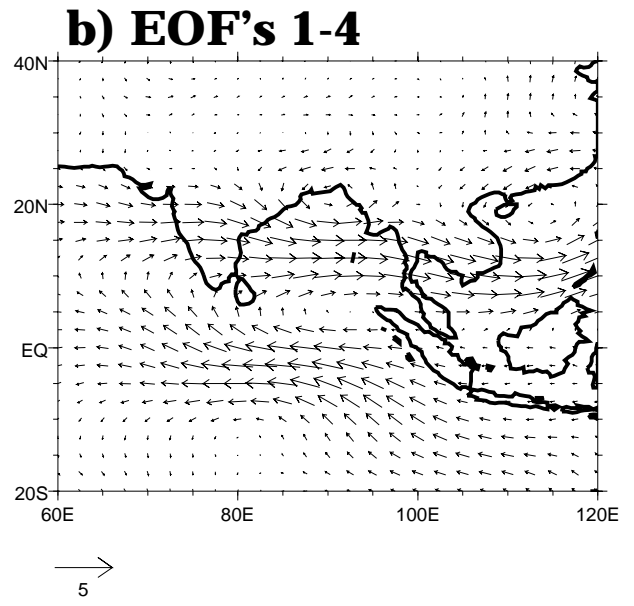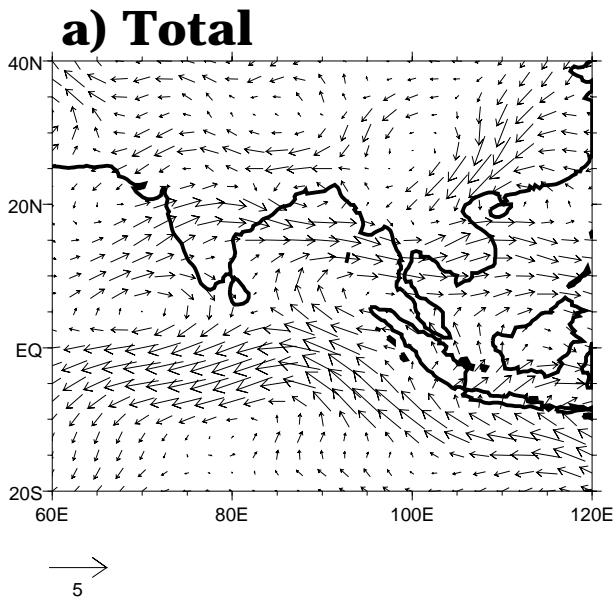

b) EOF's 1-4

c) Filtered EOF's 1-4
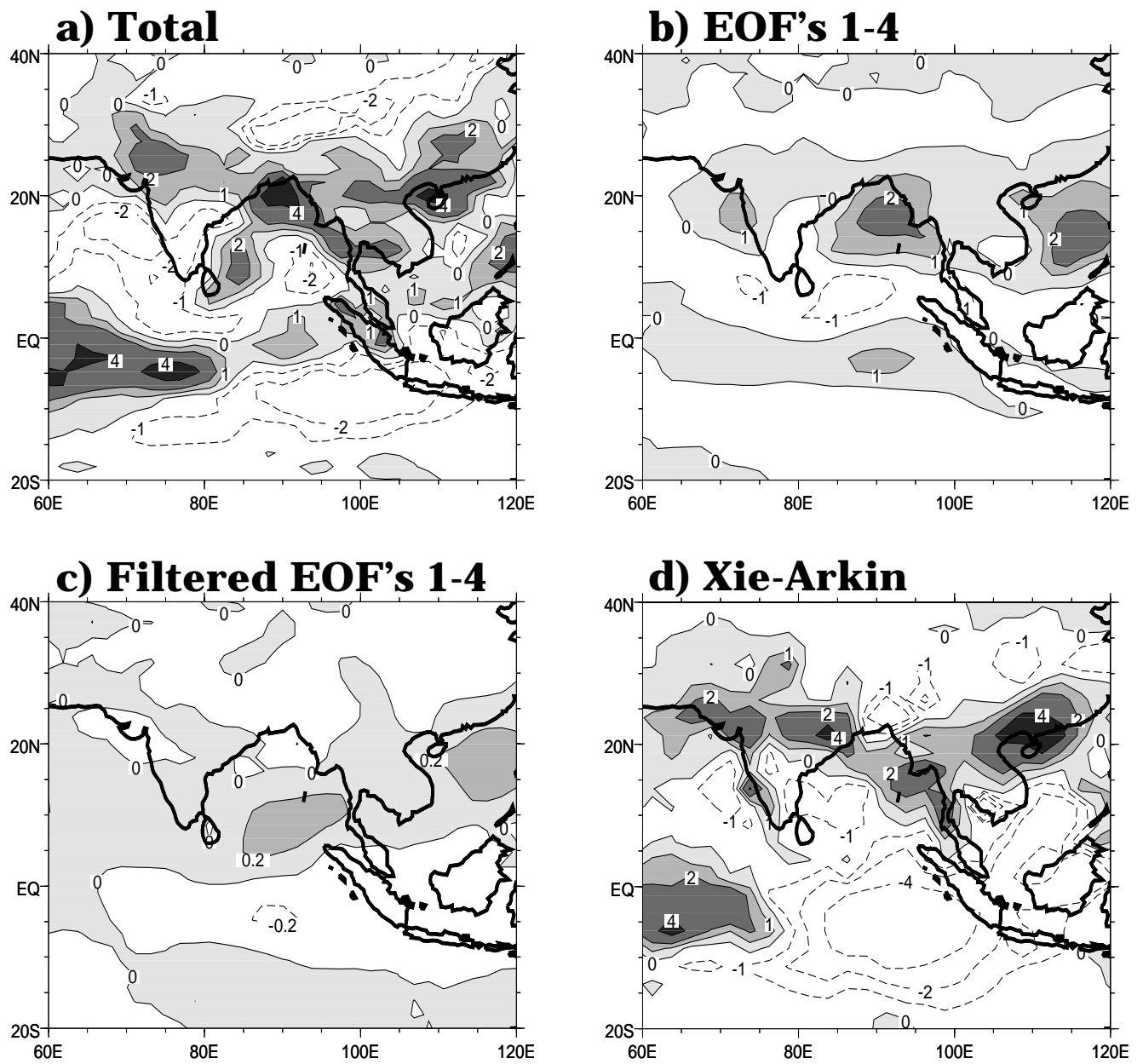

Figure 22: As Fig. 18 for 1994.

Figure 23: As Fig. 19 for 1994.

there is between the filtered rainfall reconstruction (Fig. 23c) and the observed anomalies (Fig. 23d) is fortuitous given the incorrect reconstruction of the filtered winds in Fig. 22c.

The reconstructions of the seasonal mean (June-September) 850hPa wind anomalies using the first four modes of unfiltered subseasonal variability have been successful in capturing the gross characteristics of the total seasonal anomaly. Similarly, the associated reconstructions of the rainfall anomalies are quite good considering the circuitous route through which they were produced, and the assumption that the rainfall anomalies are linearly related to the wind anomalies. Reconstructions of other years (not shown) have been equally successful. The differences between the observed and reconstructed rainfall anomalies highlight locations where the wind reconstructions failed to capture regional features in the flow. This indicates that the ASM is not dominated by a few modes of variability, and that improvement of the reconstructions may be possible through inclusion of a larger number of modes. For example, inclusion of higher order subseasonal modes that are associated with variations of the Mei-Yu front lead to an improved reconstruction of the anomalies over China (not shown). Comparison with reconstructions based on the highpass filtered data demonstrates that it is the low-frequency variations of the basic state that must be forecast.

6. Discussion and Conclusions

We have used the NCEP/NCAR reanalysis to investigate the dominant modes of subseasonal variability of the Asian summer monsoon, and we have evaluated their projection onto interannual variations of the monsoon system. First and foremost we have identified a common mode of variability that dominates the subseasonal (EOF-3/PC-3) and the interannual variations (EOF-4/PC-4) of 850hPa circulation and rainfall over India. The results indicate that the monsoon system over India is biased towards more active (break) periods during years of above (below) normal AIR. If the underlying forcing of the interannual variations of this mode can be isolated, and be shown to be predictable, then the prospect for probabilistic forecasting of Indian summer monsoon using dynamical methods will improve. Furthermore, the background state upon which the interannual variations of this mode are set is related to interdecadal variations in the Indian Ocean SST and the land-sea temperature contrast. Unfortunately, the poor observational network in the Indian Ocean provides little if any information on its subsurface structure from which to ascertain the root cause of the interdecadal variability.

In the case of the TCZ, one of the 3 modes of subseasonal variability that influences its northward propagation (EOF-2/PC-2) is systematically perturbed by ENSO. Since ENSO forecasting has reached a mature state, having moved into the realm of operational forecasting rather than experimental forecasting, this provides the basis for long-range forecasting of at least one aspect of summer monsoon. These results support the Palmer (1994) hypothesis that perturbations to otherwise chaotic phenomena can result in discernible influences on interannual timescales (although the impact is not on the leading mode, and the perturbations are not manifest as bimodality as had been suggested by simple models).

Furthermore, the analysis of highpass filtered data indicates that the aforementioned systematic pertubations require that only the slowly varying components of the climate system be forecast in order to obtain potential predictability of the Asian summer monsoon system, consistent with the earlier suggestion of Charney and Shukla (1981). This result is further supported by the reconstructions of the seasonal mean anomalies of 850hPa circulation and rainfall based on the contributions of the dominant subseasonal modes.

Even given the potential for predictability using the systematically forced modes, long-lead forecasting of the Asian summer monsoon will remain challenging for many reasons including: (1) The ENSO boundary forcing, for which there is long-range predictability of up to one-year in advance, only systematically perturbs EOF-2/PC-2. Therefore, random biases to the other subseasonal modes can either exacerbate or counteract the systematic influence caused by the ENSO boundary forcing. (2) ENSO is not a perennial occurrence, thus for the majority of years no *a priori* predisposition of the EOF-2/PC-2 will be forthcoming. (3) The first and fourth modes appear to be normal modes of the ASM since their spatial and temporal evolutions were largely unaffected by the highpass filtering. This suggests that low frequency basic state forcings are absent which might perturb these modes into preferred regimes. Thus, they introduce a substantial element of uncertainty into any long-lead forecast. (4) While the reconstructions were successful at capturing the basic structures of the 850hPa flow and the rainfall using the first four modes of subseasonal variability, the reconstructions were problematic in that they did not capture many of the regional-scale features of the seasonal mean anomalies, particularly over eastern Asia. Additionally, the reconstructed large-scale anomalies were poorly represented north of 30°N and south of the equator. Thus, a larger number of modes are necessary to improve the reconstructions since the Asian summer monsoon system is not dominated by a few modes of variability. This puts a more substantial

onus on any forecast system since the model must be able to represent a large number of modes of variability with fidelity. If numerical weather prediction models are not able to simulate such a suite of modes this would suggest that the present limitations on seasonal predictability of ASM are imposed by our limited understanding of the complex processes that govern the ocean-atmosphere-land system rather than by nature itself.

Appendix

t-test and estimation of the number of degrees of freedom

The t-test statistic was used to assess differences in the means of the probability distribution functions (PDF's). Calculation of the t-statistic requires estimates of the number of degrees of freedom for each PDF. For each summer (June-September, n=122 days) we calculate the lag 1 autocorrelation of the principal component, R1, and then conservatively estimate the number of degrees of freedom, n′, as

$$n′ \sim n(1 - R1)/(1 + R1)$$

in order to take into account serial correlation (Quenouille 1952, Wilks 1995). The sum of the number of degrees of freedom for the years over which the PDF's are calculated is then employed in assessing the statistical significance of the difference of the means of the PDF's. Our null and alternative hypotheses are:

H_0: mean1 = mean2; H_1: mean1 ≠ mean2

Given that we have no a priori knowledge of the possible perturbations to the PDF's for the extreme years, significance testing is performed at the 5% significance level using a two-tailed test. We may reject the null hypothesis at the 5% significance level if mean1-mean2 > t-statistic, and conclude at the 2.5% significance level that mean1 > mean2. Alternatively, we may reject H_0 at the 5% significance level if mean1-mean2 < -1*t-statistic, and conclude at the 2.5% significance level that mean1 < mean2 (Robbins and Van Ryzin 1975).

References

Annamalai, H., Slingo, J. M., Sperber, K. R. and Hodges, K. 1999: The mean evolution and variability of the Asian summer monsoon: comparison of ECMWF and NCEP/NCAR reanalyses. Mon. Wea. Rev., 127, 1157-1186.

Brankovic, C. and Palmer, T. N. 1999: Seasonal skill and predictability of ECMWF PROVOST ensembles. Q. J. Roy. Meteorol. Soc. (submitted).

Charney, J. G. and Shukla, J. 1981: Predictability of monsoons. Chapter in "Monsoon Dynamics", Cambridge University Press, pp. 99-110.

Fennessy, M. J. and Shukla, J. 1994: GCM simulations of active and break monsoon periods. Proc. of the International Conference on Monsoon Variability and Prediction, Trieste, Italy, WCRP-84, WMO/TD-No. 619, Vol. 2, 576-585.

Ferranti, L., Slingo, J. M., Palmer, T. N. and Hoskins, B. J. 1997: Relations between interannual and intraseasonal monsoon variability as diagnosed from AMIP integrations. Q. J. R. Meteorol. Soc., 123, 1323-1357.

Gadgil, S. 1988: Recent advances in monsoon research with particular reference to the Indian monsoon. Australia Meteorological Magazine, 36, 193-204.

Gadgil, S. and Asha, G. 1992: Intraseasonal variation of the summer monsoon I: observational aspects. J. Meteorol. Soc. Japan, 70, 517-527.

Goswami, B. N. 1994: Dynamical predictability of seasonal monsoon rainfall: problems and prospects. Proc. Ind. Nat. Sci. Acad., 60A, 101-120.

Goswami, B. N., Krishnamurti, V. and Annamalai, H. 1999: A broad-scale circulation index for the interannual variability of the Indian summer monsoon. Q. J. Roy. Meteorol. Soc., 125, 611-633.

Goswami, B. N., Sengupta, D. and Suresh Kumar, G. 1998: Intraseasonal oscillations and interannual variability of surface winds over the Indian monsoon region. Proc. Indian Acad. Sci. (Earth Planet. Sci.), 107, 45-64.

Ju, J. and Slingo, J. M. 1995: The Asian Summer Monsoon and ENSO. Q. J. R. Meteorol. Soc., 121, 1133-1168.

Kalnay, E., Kanamitsu, M., Kistler, R., Collins, W. Deaven, D., Gandin, L., Iredell, M., Saha, S., White, G., Woollen, J., Zhu, Y., Chelliah, M., Ebisuzaki, W., Higgins, W., Janowiak, J., Mo, K. C., Ropelewski, C., Wang, J., Leetma, A., Reynolds, R., Jenne R. and Joseph, D. 1996: The NCEP/NCAR 40-year reanalysis project. Bull. Amer. Met. Soc., 77, 437-471.

Kiladis, G. N. and Sinha, S. K. 1991: ENSO, monsoon and drought in India. in *Tele-connections linking worldwide climate anomalies*. Glantz, M. H. Katz, R. W., & Nicholls, N. (editors), Cambridge University Press, Cambridge, UK, 431-458.

Krishna Kumar, K., Soman, M. K. and Rupa Kumar, K. 1995: Seasonal forecasting of Indian summer monsoon rainfall. Weather, 50, 449-467.

Krishnamurti, T. N. and Bhalme, H. N. 1976: Oscillations of the monsoon system. part 1. observational aspects. J. Atmos. Sci., 33, 1937-1954.

Krishnamurti, T. N., Bedi, H. S. and Subramaniam, M. 1989: The summer monsoon of 1987. J. Clim., 2, 321-340.

Lau, K.-M. and Chan, P. H. 1986: Aspects of the 40-50 day oscillation during northern summer as inferred from outgoing longwave radiation. Mon. Wea. Rev., 114, 1354-1367.

Lorenz, E. N. 1963: Deterministic non-periodic flow. J. Atmos. Sci., 20, 130-141.

McPhaden, M. J. 1999: Genesis and evolution of the 1997-98 El Niño. Science, 283, 950-954.

Mo, K. C. and Higgins, R. W. 1996: Large-scale atmospheric moisture transport as evaluated in the NCEP/NCAR and the NASA/DAO reanalyses. J. Clim., 9, 1531-1545.

Murakami, M. 1976: Analysis of summer monsoon fluctuations over India. J. Meteorol. Soc. Japan, 54, 15-31.

Palmer, T. N. 1994: Chaos and predictability in forecasting the monsoon. Proc. Indian Nat. Sci. Acad., 60A, 57-66.

Palmer, T. N. 1999: A nonlinear perspective on climate prediction. J. Clim. 12, 575-591.

Pan, H. L. and Mahrt., L. 1987: Interaction between soil hydrology and boundary layer developments. Bound. Layer Met., 38, 185-202.

Pan, H. L. and Wu, W. S. 1994: Implementing a mass-flux convection parameterization package for the NMC medium-range forecast model. Proceedings of the Tenth Conference on Numerical Weather Prediction, Portland/Oregon, pp. 96-98.

Parthasarathy, B., Munot A. A. and Kothawale, D. R. 1994: All-India monthly and seasonal rainfall series: 1871-1993. Theoretical and Applied Climatology, 49, 217-224.

Quenouille, M. A. 1952: Associated Measurements., Butterworths, 242pp.

Ramamurthy, K., 1969: Some aspects of the break in the Indian southwest monsoon during July and August. *Forecasting manual* (available from India Meteorological Department, Lodi Road, New Delhi), Part IV-18.3.

Ramanadham, R., Rao, P. V. and Patnaik, J. K. 1973: Break in the Indian summer monsoon. Pure Appl. Geophys., 104, 635-647.

Robbins, H. and Van Ryzin, J. 1975: Introduction to Statistics. Science Research Associates, Chicago, IL, USA. 427pp.

Rowell, D. P., Folland, C. K., Maskell, K. and Ward, M. N. 1995: Variability of summer rainfall over tropical North Africa (1906-92): Observations and modelling. Q. J. R. Meteorol. Soc., 121, 669-704.

Sikka, D. R. 1980: Some aspects of the large-scale fluctuations of summer monsoon rainfall over India in relation to fluctuations in the planetary and regional scale circulation parameters. Proceedings of the Indian Academy of Science (Earth and Planet. Sci.), 89, 179-195.

Sikka, D. R. and Gadgil, S. 1980: On the maximum cloud zone and the ITCZ over Indian longitudes during the Southwest Monsoon. Mon. Wea. Rev., 108, 1840-1853.

Slingo, J. M. 1987: The development and verification of a cloud prediction scheme for the ECMWF model. Q. J. R. Meteorol. Soc., 113, 899-927.

Slingo, J. M. 1998: The summer monsoon and its variability. in "Beyond El Niño: Decadal Variability in the Climate System," ed. A. Navarra, Springer.

Sperber, K. R. and Palmer, T. N. 1996: Interannual tropical rainfall variability in general circulation model simulations associated with the Atmospheric Model Intercomparison Project. J. Climate, 9, 2727-2750.

Stendel, M. and Arpe, K. 1997: Evaluation of the hydrological cycle in reanalyses and observations. Report No. 228, Max-Planck-Institut für Meteorologie, Hamburg, Germany.

Swaminathran, M. S. 1987: Abnormal monsoons and economic consequences: the Indian experiment. in *Monsoons*. Fein, J. S., & Stephens, P. L. (editors), 121-134.

Trenberth, K. E and Guillemot, C. J. 1998: Evaluation of the atmospheric moisture and hydrological cycle in the NCEP/NCAR reanalyses. Clim. Dyn., 14, 213-231.

Vincent, D. G., Fink, A. Schrage, J. M. and Speth, P. 1998: High- and low-frequency intraseasonal variance of OLR on annual and ENSO timescales. J. Clim., 11, 968-986.

Walker, G. T. and Bliss, E. W. 1932: World weather, V. Mem. Roy. Meteorol. Soc., 4, 53-84.

Wang, B. and Rui, H. 1990: Synoptic climatology of transient tropical intraseasonal convection anomalies: 1975-1985. Meteorol. Atmos. Phys., 44, 43-61.

WCRP, 1992: Simulation of interannual and intraseasonal monsoon variability. WMO/TD-No. 470, Geneva, Switzerland, 185pp.

WCRP, 1993: Simulation and prediction of monsoons: Recent results. WMO/TD-No. 546, Geneva, Switzerland, 73pp.

Webster, P. J. and Yang, S. 1992: Monsoon and ENSO: Selectively interactive systems Q. J. R. Meteorol. Soc., 118, pp. 877-926.

Webster, P. J., Magana, V. O. Palmer, T. N., Shukla, J., Tomas, R. A. Yanai, M. and Yasunari, T. 1998: The Monsoon: Processes, predictability and prediction. J. Geophys. Res., 103, 14,451-14510.

Wilks, D. S. 1995: Statistical Methods in the Atmospheric Sciences: An Introduction. Academic Press, San Diego, CA, USA, 467pp.

Xie, P and Arkin, P. 1996: Analyses of global monthly precipitation using gauge observations, satellite estimates and numerical model predictions. J. Clim., 9, 840-858.

Xie, P and Arkin, P. 1997: Global precipitation: A 17-year monthly analysis based on gauge observations, satellite estimates, and numerical model outputs. Bull. Amer. Meteorol. Soc., 78, 2539-2558.

Yasunari, T. 1979: Cloudiness fluctuations associated with the northern hemisphere summer monsoon. J. Meteorol. Soc. Japan, 57, 227-242.

Yasunari, T. 1980: A quasi-stationary appearance of 30 to 40 day period in cloudiness fluctuations during the summer monsoon over India. J. Meteorol. Soc. Japan, 58, 225-229.

Yasunari, T. 1981: Structure of an Indian summer monsoon system with around 40-day period. J. Meteorol. Soc. Japan, 59, 336-354.